

OUTP-96-56P
hep-th/9609237

Revised Version

January 1, 2018

Curvature Matrix Models for Dynamical Triangulations and the Itzykson-Di Francesco Formula

Richard J. Szabo^{1,2} and John F. Wheater³

*Department of Physics, Theoretical Physics
University of Oxford
1 Keble Road, Oxford OX1 3NP, U.K.*

Abstract

We study the large- N limit of a class of matrix models for dually weighted triangulated random surfaces using character expansion techniques. We show that for various choices of the weights of vertices of the dynamical triangulation the model can be solved by resumming the Itzykson-Di Francesco formula over congruence classes of Young tableau weights modulo three. From this we show that the large- N limit implies a non-trivial correspondence with models of random surfaces weighted with only even coordination number vertices. We examine the critical behaviour and evaluation of observables and discuss their interrelationships in all models. We obtain explicit solutions of the model for simple choices of vertex weightings and use them to show how the matrix model reproduces features of the random surface sum. We also discuss some general properties of the large- N character expansion approach as well as potential physical applications of our results.

¹Work supported in part by the Natural Sciences and Engineering Research Council of Canada.

²email address: r.szabo1@physics.oxford.ac.uk

³email address: j.wheater1@physics.oxford.ac.uk

1 Introduction

The statistical mechanics of random surfaces has been of much interest over the years in the random geometry approach to two-dimensional quantum gravity and lower dimensional string theory. These models can be solved non-perturbatively by viewing discretized Riemann surfaces as Feynman graphs of $N \times N$ matrix models (see [1] for a review). The large- N limit of the matrix model exhibits phase transitions which correspond to the continuum limit of the dynamically triangulated random surface model and whose large- N expansion coincides with the genus expansion of the string theory. In this paper we will study a class of matrix models originally proposed by Das et al. [2] in which the weighting of the coordination numbers of vertices (describing intrinsic curvature) of the dynamical triangulation of the surface can be varied. These “curvature” matrix models have been solved exactly in the large- N limit for a Penner interaction potential by Chekhov and Makeenko [3], and more recently for an arbitrary potential by Kazakov, Staudacher and Wynter [4, 5] using group character expansion methods.

There are many problems of interest which could be solved from the large- N limit of such matrix models. Foremost among these are questions related to the quantum geometry and fractal structure of the surfaces which contribute to the string partition function. For instance, the string theory ceases to make sense for string embedding dimensions $D > 1$. However, there is no obvious pathological reason for the existence of a barrier in the statistical mechanical model at $D = 1$, and it has been suggested [6] that the statistical mechanical model evolves into a different geometrical phase for $D > 1$, for instance a branched polymer (tree-like) phase, rather than the stringy (intrinsically two-dimensional) phase. It was argued in [2] that curvature matrix models can represent such a transition by variation of the weighting of the vertex coordination numbers. The trees are to be thought of as connecting two-dimensional baby universes together in each of which the usual $D < 1$ behaviour is exhibited (see [7] for a review). Another problem is the exact solution of two-dimensional quantum gravity with higher curvature counterterms added to the action and the associated problem of the existence of a phase transition from the gravitational phase to a flat phase of the same string theory. By varying the vertex coordination numbers of a random lattice to a flat one, the genus zero problem can be obtained as the non-perturbative large- N solution of an appropriate curvature matrix model and it was demonstrated in [8] that there is no such phase transition. Besides these problems, there are many other interesting physical situations which require control over the types of surfaces that contribute to the random sum.

The main subject of this paper is the curvature matrix model defined by the partition function

$$Z_H[\lambda, t_q^*] = (2\pi\lambda)^{-N^2/2} \int dX \ e^{-\frac{N}{2\lambda} \text{tr } X^2 + N \text{tr } V_3(XA)} \quad (1.1)$$

where

$$V_3(XA) = \frac{1}{3}(XA)^3 \quad (1.2)$$

and the integration is over the space of $N \times N$ Hermitian matrices X with A an invertible $N \times N$ external matrix. The Feynman diagram expansion of (1.1) can be written symbolically as

$$Z_H[\lambda, t_q^*] = \sum_{G_3} \prod_{v_q^* \in G_3} \left(\lambda^{q/2} t_q^* \right)^{\mathcal{N}(v_q^*)} \quad (1.3)$$

where the sum is over all fat-graphs G_3 made up of 3-point vertices, the weight associated to a vertex v_q^* of the lattice dual to G_3 of coordination number q is

$$t_q^* = \frac{1}{q} \frac{\text{tr}}{N} A^q \quad , \quad (1.4)$$

and $\mathcal{N}(v_q^*)$ is the number of such vertices in G_3 . This matrix model therefore assigns a weight t_q^* whenever q 3-point vertices bound a face of the associated surface discretization, and it thus allows one to control the local intrinsic curvature $R_q = \pi(6 - q)/q$ of the dynamical triangulation. We will examine the structure of the solution at large- N when these dual weights are arranged so that the only triangulations which contribute to the sum in (1.3) are those whose vertices have coordination numbers which are multiples of three.

There are several technical and physical reasons for studying such a model. The method of exact solution developed in [4, 5] is based on a treatment of the large- N limit of the Itzykson-Di Francesco character expansion formula [9]. This formula is most naturally suited to matrix models of random surfaces whose vertices have even coordination numbers, and therefore the analysis in [4, 5, 8] was restricted to such situations. In the following we will show that the large- N limit of the Itzykson-Di Francesco formula for the curvature matrix model (1.1) can be used provided that one arranges the group character sum carefully. This arrangement reflects the discrete symmetries of the triangulation model that are not present in the models with vertices of only even coordination number. We shall see that this solution of the curvature matrix model actually implies a graph theoretical equivalence between the dynamically triangulated model and certain even coordination number models which were studied in [4, 5]. We will also show how to map the Hermitian matrix model (1.1) onto a complex one whose character expansion is especially suited to deal with coordination numbers which are multiples of three and whose observables are in a one-to-one correspondence with those of the even coordination number matrix models. As a specific example, we solve the model explicitly for a simple power law variation of the vertex weights (1.4) which agrees with expected results from the random surface sums and which provides explicit insights into the non-perturbative behaviour of observables of the curvature matrix model (1.1), and also into the phase structure of the Itzykson-Zuber model [10] which is related to higher-dimensional Hermitian matrix models [1, 7, 11]. There are several physical situations which are best

described using such dynamical triangulations [6]. The analysis which follows also applies to quite general odd coordination number models and establishes a non-trivial application of the techniques developed in [4, 5].

The organization of this paper is as follows. In section 2 we derive the character expansion of the matrix model (1.1) and discuss the structure of the Itzykson-Di Francesco formula in this case. We also show that certain symmetry assumptions that are made agree with the mapping of the model onto a complex curvature matrix model which demonstrates explicitly how the character sum should be taken. In section 3 we discuss the large- N saddle point solutions of these matrix models. We show that the Itzykson-Di Francesco formula implies non-trivial correspondences between the Feynman graphs of the matrix model (1.1) and those of some models of random surfaces with even coordination numbers. We also establish this correspondence more directly using graph theory arguments. We analyse the critical behaviour of the matrix model when all vertices are weighted equally and discuss the various relations that exist among observables of the matrix models. We also demonstrate explicitly using the Wick expansion of (1.1) that the large- N solution of section 2 is indeed correct. In section 4 we examine a simple situation where the dual vertices of the dynamical triangulation are not weighted equally. We show how this affects the large- N saddle-point solution of the matrix model and thereby establish the validity of our solution for generic choices of the vertex coupling constants. Our results here may also be relevant to the study of phase transitions in the Itzykson-Zuber model [7, 11]. In section 5 we briefly discuss the difficult problems which occur when dealing with matrix models that admit complex-valued saddle-points of the Itzykson-Di Francesco formula, and section 6 contains some concluding remarks and potential physical applications of our analysis.

2 Large- N Character Expansion of the Partition Function

We begin by describing the character expansion method for solving the matrix model (1.1) in the large- N limit [4, 5]. The external field A in (1.1) explicitly breaks the invariance of the model under unitary transformations $X \rightarrow UXU^\dagger$ which diagonalize the Hermitian matrix X . Thus, unlike the more conventional matrix models with $A = \mathbf{1}$ for which the dual vertices v_q^* are all weighted equally [1], the partition function (1.1) cannot be written as a statistical theory of the eigenvalues of X . The number of degrees of freedom can still, however, be reduced from N^2 to N by expanding the invariant function $e^{\frac{N}{3} \text{tr}(XA)^3}$ in characters of the

Lie group $GL(N, \mathbb{C})$ as [4]

$$e^{\frac{N}{3} \text{tr}(XA)^3} = c_N \sum_{\{h_i\}} \mathcal{X}_3[h] \chi_{\{h_i\}}(XA) \quad (2.1)$$

where c_N denotes an irrelevant numerical constant and

$$\mathcal{X}_3[h] = \left(\frac{N}{3}\right)^{\frac{1}{3} \sum_{i=1}^N h_i} \prod_{\epsilon=0,1,2} \frac{\Delta[h^{(\epsilon)}]}{\prod_{i=1}^{N/3} \left(\frac{h_i^{(\epsilon)} - \epsilon}{3}\right)!} \text{sgn} \left[\prod_{0 \leq \epsilon_1 < \epsilon_2 \leq 2} \prod_{i,j=1}^{N/3} (h_i^{(\epsilon_2)} - h_j^{(\epsilon_1)}) \right] \quad (2.2)$$

The sum in (2.1) is over unitary irreducible representations of $GL(N, \mathbb{C})$. They are characterized by their Young tableau weights $\{h_i\}_{i=1}^N$ which are increasing non-negative integers, $0 \leq h_i < h_{i+1}$, and are defined by $h_i = i - 1 + b_i$ where b_i is the number of boxes in row i of the associated Young tableau. Because of the 3-valence coupling on the left-hand side of (2.1), the sum is supported on those weights which can be factored into three groups of equal numbers of integers $h_i^{(\epsilon)}$, $i = 1, \dots, \frac{N}{3}$, where $\epsilon = 0, 1, 2$ labels their congruence classes modulo 3. The $GL(N, \mathbb{C})$ characters can be written using the Weyl character formula as

$$\chi_{\{h_i\}}(Y) = \frac{\det_{k,\ell}[y_k^{h_\ell}]}{\Delta[y]} \quad (2.3)$$

where $y_i \in \mathbb{R}$ are the eigenvalues of the Hermitian matrix Y and

$$\Delta[y] = \prod_{i < j} (y_i - y_j) = \det_{k,\ell}[y_k^{\ell-1}] \quad (2.4)$$

is the Vandermonde determinant.

Substituting (2.1) into (1.1) and diagonalizing X , the integration over unitary degrees of freedom can be carried out explicitly using the Schur orthogonality relations for the characters. The resulting expression is a statistical mechanics model in Young tableau weight space which is a special case of the Itzykson-Di Francesco formula [4, 9]

$$Z_H[\lambda, t_q^*] = c_N \sum_{h=\{h^e, h^o\}} \frac{\prod_{i=1}^{N/2} (h_i^e - 1)!! h_i^o!!}{\prod_{i,j=1}^{N/2} (h_i^e - h_j^o)} \mathcal{X}_3[h] \chi_{\{h\}}(A) \left(\frac{\lambda}{N}\right)^{-\frac{1}{4}N(N-1)+\frac{1}{2}\sum_{i=1}^{N/2}(h_i^e+h_i^o)} \quad (2.5)$$

The sum in (2.5) is restricted to the even representations of $GL(N, \mathbb{C})$, i.e. those with Young tableau weights which split into an equal number of even and odd integers h_i^e and h_i^o , $i = 1, \dots, \frac{N}{2}$. This restriction arises because of the Gaussian integration over the eigenvalues $x_i \in (-\infty, \infty)$ of the matrix X [4]. Because of (2.2), these weights must also split equally into their congruence classes modulo 3. The partition function (2.5) depends on only N degrees of freedom (the Young tableau weights h_i) and thus the curvature matrix model (1.1) is formally solvable in the large- N limit.

For definiteness, we consider the matrix model of dually weighted discretized surfaces for which the only graphs contributing in (1.3) are those triangulations which have $3m$, $m =$

$1, 2, \dots$, nearest-neighbour sites to each vertex. This means that the vertex weights t_q^* in (1.4) are non-vanishing only when q is a multiple of three. To realize this explicitly in the matrix model (1.1), we take the external matrix A to be of the block form

$$A = A^{(3)} \equiv \begin{pmatrix} \bar{A}^{1/3} & 0 & 0 \\ 0 & \omega_3 \bar{A}^{1/3} & 0 \\ 0 & 0 & \omega_3^2 \bar{A}^{1/3} \end{pmatrix} \quad (2.6)$$

where $\omega_3 \in \mathbb{Z}_3$ is a non-trivial cube root of unity and $\bar{A}^{1/3}$ is an invertible $\frac{N}{3} \times \frac{N}{3}$ Hermitian matrix. The character (2.3) can then be evaluated explicitly to get [4]

$$\chi_{\{h\}}(A^{(3)}) = \chi_{\left\{ \frac{h^{(0)}}{3} \right\}}(\bar{A}) \chi_{\left\{ \frac{h^{(1)}-1}{3} \right\}}(\bar{A}) \chi_{\left\{ \frac{h^{(2)}-2}{3} \right\}}(\bar{A}) \operatorname{sgn} \left[\prod_{0 \leq \epsilon_1 < \epsilon_2 \leq 2} \prod_{i,j=1}^{N/3} (h_i^{(\epsilon_2)} - h_j^{(\epsilon_1)}) \right] \quad (2.7)$$

and the statistical sum (2.5) becomes

$$Z_H[\lambda, t_q^*] = c_N \lambda^{-\frac{1}{4}N(N-1)} \sum_{h=\{h^e, h^o\}} \frac{\prod_i (h_i^e - 1)!! h_i^o!!}{\prod_{i,j} (h_i^e - h_j^o)} \prod_{\epsilon=0,1,2} \left(\frac{\Delta[h^{(\epsilon)}] \chi_{\left\{ \frac{h^{(\epsilon)}-\epsilon}{3} \right\}}(\bar{A})}{\prod_i \left(\frac{h_i^{(\epsilon)}-\epsilon}{3} \right)!} \right) \times e^{\sum_i h_i [\frac{1}{2} \log(\frac{\lambda}{N}) + \frac{1}{3} \log(\frac{N}{3})]} \quad (2.8)$$

Notice that the sign factors from (2.2) and (2.7) cancel each other out in (2.8).

To treat the large- N limit, we assume that at $N = \infty$ the sum over representations in (2.8) becomes dominated by a single, most-probable Young tableau $\{h_i\}$. The problem that immediately arises is that the groupings of the Young tableau weights in (2.8) into equal numbers of even and odd integers and into equal numbers of mod 3 congruence elements need not occur symmetrically. There does not appear to be any canonical way to split the weights up and distribute them in the appropriate way. However, it is natural to assume, by the symmetry of the weight distributions in (2.8), that the saddle-point localizes around that configuration with equal numbers of even and odd weights, *each* set of which groups with equal numbers into their mod 3 congruence classes $h_i^{e(\epsilon)}$ and $h_i^{o(\epsilon)}$, $i = 1, \dots, \frac{N}{6}$. It is also natural, by symmetry again, to further assume that although the different sets of weights $h_i^{e(\epsilon)}, h_i^{o(\epsilon)}$ do not factorize and decouple from each other, the groupings of the weights into even and odd mod 3 congruence classes are distributed in the same way. We therefore assume this symmetrical splitting in (2.8) and write the statistical sum over the mod 3 congruence classes of weights $h_i^{(\epsilon)}$. We also make the additional assumption that the product of weights from two different congruence class groupings contributes the same in the large- N limit as the Vandermonde determinant for a single grouping, i.e. that

$$\prod_{i,j} (h_i^{(\epsilon_2)} - h_j^{(\epsilon_1)}) = \prod_{i \neq j} (h_i^{(\epsilon_1)} - h_j^{(\epsilon_1)}) \quad (2.9)$$

for $\epsilon_2 \neq \epsilon_1$. As we shall see, these symmetrical grouping assumptions are indeed valid and lead to the appropriate solution of the curvature matrix model (1.1) at large- N .

We now rescale $h_i \rightarrow N \cdot h_i$ in (2.8), simplify the factorials for large- N using the Stirling approximations $h!! \sim e^{h(\log h - 1)/2}$ and $h! \sim e^{(h+\frac{1}{2}) \log h - h}$, and apply the above symmetry assumption retaining only the leading planar (order $1/N$) contributions to (2.8). After some algebra, the partition function (2.8) for the symmetrically distributed weights $h^{(0)}$ in the large- N limit can be written as

$$Z_H^{(0)} \sim \sum_{h^{(0)}} e^{N^2 S_H[h^{(0)}]} \quad (2.10)$$

where the effective action is

$$\begin{aligned} S_H[h^{(0)}] = & -\frac{1}{4} \log \lambda + \frac{3}{2N^2} \sum_{i < j}^{N/3} \log(h_i^{(0)} - h_j^{(0)}) + \frac{1}{2N} \sum_{i=1}^{N/3} h_i^{(0)} \left[2 \log \lambda + \log(\lambda h_i^{(0)}) - 1 \right] \\ & + \frac{3}{N^2} \log I \left[\frac{Nh^{(0)}}{3}, \bar{A} \right] \end{aligned} \quad (2.11)$$

and we have introduced the Itzykson-Zuber integral [10]

$$I[h^{(0)}, \bar{A}] \equiv \int_{U(N/3)} dU \ e^{\sum_{i,j} h_i^{(0)} \alpha_j |U_{ij}|^2} = \chi_{\{h^{(0)}\}}(\bar{A}) \frac{\Delta[a]}{\Delta[h^{(0)}] \Delta[\alpha]} \quad (2.12)$$

where a_i are the eigenvalues of the matrix \bar{A} and $\alpha_i \equiv \log a_i$. In arriving at (2.10) we have used the Vandermonde determinant decomposition

$$\Delta[h^{(\epsilon)}] = \Delta[h^{e(\epsilon)}] \Delta[h^{o(\epsilon)}] \prod_{i,j=1}^{N/6} (h_i^{e(\epsilon)} - h_j^{o(\epsilon)}) \quad (2.13)$$

and ignored irrelevant terms which are independent of λ and the h 's.

In the case of the even coordination number models studied in [4, 5, 8] the natural weight distribution to sum over in the Itzykson-Di Francesco formula (2.5) is that of the original even representation restriction (see subsection 3.1). In our case the natural weight distribution appears to be that of the mod 3 congruence classes. However, in contrast to the even coordination number models, there is no way to justify this from the onset. We shall see later on that the appropriate distribution for the Itzykson-Di Francesco formula at large- N is essentially determined by the discrete symmetries of the given curvature matrix model. Some evidence for the validity of this assumption comes from comparing the Hermitian model here with the *complex* curvature matrix model

$$Z_C[\lambda, t_q^*] = (2\pi\lambda)^{-N^2} \int d\phi \, d\phi^\dagger \, e^{-\frac{N}{\lambda} \text{tr } \phi^\dagger \phi - \frac{1}{3} \text{tr}(\phi A \phi^\dagger B)^3} \quad (2.14)$$

where the integration is now over the space of $N \times N$ complex-valued matrices ϕ , and B is another external $N \times N$ invertible matrix. Again one can expand the invariant, cubic

interaction term as in (2.1) and the character expansion of (2.14) is [12]

$$Z_C[\lambda, t_q^*] = c_N \sum_{h=\{h^{(\epsilon)}\}} \frac{\prod_{i=1}^N h_i!}{\Delta[h]} \chi_{\{h\}}(A) \chi_{\{h\}}(B) \mathcal{X}_3[h] \left(\frac{\lambda}{N}\right)^{-\frac{1}{2}N(N-1)+\sum_i h_i} \quad (2.15)$$

Now the Gaussian integration over the eigenvalues of the positive definite Hermitian matrix $\phi^\dagger \phi$ goes over $[0, \infty)$ and so there is no restriction to even and odd weights in (2.15), only the restriction to mod 3 congruence classes because of the 3-valence coupling. If we take $B = \mathbf{1}$, so that $\chi_{\{h\}}(B) \propto \Delta[h]$, and use the decomposition (2.6), then the character expansion (2.15) becomes

$$Z_C[\lambda, t_q^*] = c_N \lambda^{-\frac{1}{2}N(N-1)} \sum_{h=\{h^{(\epsilon)}\}} \prod_{i=1}^N h_i! \prod_{\epsilon=0,1,2} \frac{\Delta[h^{(\epsilon)}]}{\prod_i \left(\frac{h_i^{(\epsilon)} - \epsilon}{3}\right)!} \chi_{\left\{\frac{h^{(\epsilon)} - \epsilon}{3}\right\}}(\bar{A}) e^{\sum_i h_i^{(\epsilon)} [\log(\frac{\lambda}{N}) + \frac{1}{3} \log(\frac{N}{3})]} \quad (2.16)$$

Thus in this case the congruence classes of weights completely factorize, and we can now naturally assume that the $N = \infty$ configuration of weights is distributed equally into these three classes. In this sense, the complex matrix model (2.14) is a better representative of the dually-weighted triangulated random surface sum, because one need not make any ad-hoc assumptions about the weight distribution. The character expansion (2.16) suggests that the correct statistical distribution for the dynamical triangulation model at large- N is over $h_i^{(\epsilon)}$, as was assumed above, and we shall discuss the explicit relationship between these Hermitian and complex matrix models in the next section. We now rescale $h_i \rightarrow N \cdot h_i$ and simplify (2.16) for large- N as for the Hermitian model. After some algebra, the partition function (2.16) for the symmetrically distributed weights $h^{(0)}$ in the large- N limit can be written as

$$Z_C^{(0)} \sim \sum_{h^{(0)}} e^{N^2 S_C[h^{(0)}]} \quad (2.17)$$

where the effective action is

$$S_C[h^{(0)}] = -\frac{1}{2} \log \lambda + \frac{6}{N^2} \sum_{i < j}^{N/3} \log(h_i^{(0)} - h_j^{(0)}) + \frac{2}{N} \sum_{i=1}^{N/3} h_i^{(0)} [\log(\lambda^{3/2} h_i^{(0)}) - 1] + \frac{3}{N^2} \log I \left[\frac{N h^{(0)}}{3}, \bar{A} \right] \quad (2.18)$$

3 Saddle-point Solutions

If the characteristic h 's which contribute to the sum in (2.10) are of order 1, then the large- N limit of the Itzykson-Di Francesco formula can be found using the saddle-point approximation. The attraction or repulsion of the λ -dependent terms in (2.8) is compensated by the Vandermonde determinant factors, so that, in spite of the unsymmetrical grouping of Young tableau

weights that occurs, the partition function is particularly well-suited to a usual saddle-point analysis in the large- N limit. In this section we shall see that the symmetry assumptions made above give a well-posed solution of the matrix model at $N = \infty$. The partition functions (1.1) and (2.14) are dominated at large- N by their saddle points which are the extrema of the actions in (2.11) and (2.18). In what follows we shall determine the saddle-point solutions of both the Hermitian and complex matrix models and use them to examine various properties of the random surface sum.

3.1 Hermitian Model

To find the saddle-point solution of the Hermitian matrix model, we minimize the action (2.11) with respect to the Young tableau weights. Then the stationary condition $\frac{\partial S_H}{\partial h_i^{(0)}} = 0$ leads to the saddle-point equation

$$\frac{3}{N} \sum_{\substack{j=1 \\ j \neq i}}^{N/3} \frac{1}{h_i^{(0)} - h_j^{(0)}} = -\log(\lambda^3 h_i^{(0)}) - 2\mathcal{F}(h_i^{(0)}) \quad (3.1)$$

where we have introduced the Itzykson-Zuber correlator

$$\mathcal{F}(h_i^{(0)}) = 3 \frac{\partial \log I[h^{(0)}/3, \bar{A}]}{\partial h_i^{(0)}} \quad (3.2)$$

To solve (3.1), we assume that at large- N the Young tableau weights $h_i^{(0)}$, $i = 1, \dots, \frac{N}{3}$, become distributed on a finite interval $h \in [0, a]$ on the real line and introduce the normalized spectral density $\rho_H(h) \equiv \frac{dx}{dh(x)}$, where $h(x) \in [0, a]$ is a non-decreasing differentiable function of $x \in [0, 1]$ with $h(3i/N) = N \cdot h_i^{(0)}$. Discrete sums over $h_j^{(0)}$ are then replaced with integrals over h by the rule $\frac{3}{N} \sum_{j=1}^{N/3} \rightarrow \int_0^a dh$. Notice that since the h_i 's are increasing integers, we have $0 \leq \rho_H(h) \leq 1$, and so the spectral distribution is trivial, $\rho_H(h) = 1$, on some sub-interval $[0, b]$ with $0 < b \leq 1 \leq a$ [13]. The saddle-point equation (3.1) then becomes an integral equation for the spectral density,

$$\int_b^a dh' \frac{\rho_H(h')}{h - h'} = -\log(\lambda^3 h) - \log\left(\frac{h}{h - b}\right) - 2\mathcal{F}(h) \quad , \quad h \in [b, a] \quad (3.3)$$

where we have saturated the spectral distribution function at its maximum value $\rho_H(h) = 1$ on $[0, b]$. The saddle-point solution of the matrix model can thus be determined as the solution of the Riemann-Hilbert problem for the usual resolvent function

$$\mathcal{H}_H(h) = \left\langle \frac{3}{N} \sum_{i=1}^{N/3} \frac{1}{h - h_i^{(0)}} \right\rangle = \int_0^a dh' \frac{\rho_H(h')}{h - h'} \quad (3.4)$$

which is analytic everywhere in the complex h -plane away from the support interval $[0, a]$ of ρ_H where it has a branch cut. The discontinuity of the resolvent across this cut determines the spectral density by

$$\mathcal{H}_H(h \pm i0) = \oint_0^a dh' \frac{\rho_H(h')}{h - h'} \mp i\pi\rho_H(h) \quad , \quad h \in [0, a] \quad (3.5)$$

In contrast to the more conventional Hermitian one-matrix models [1], the Riemann-Hilbert problem (3.3) involves the unknown Itzykson-Zuber correlator $\mathcal{F}(h)$ which must be determined separately in the large- N limit. As shown in [4, 5], it is determined by the vertex couplings (1.4) through the contour integral

$$q\tilde{t}_q^* \equiv 3qt_{3q}^* = 3\frac{\text{tr}}{N}\bar{A}^q = \frac{1}{q}\oint_{\mathcal{C}} \frac{dh}{2\pi i} e^{q(\mathcal{H}_H(h) + \mathcal{F}(h))} \quad , \quad q \geq 1 \quad (3.6)$$

where the closed contour \mathcal{C} encircles the support of the spectral function $\rho_H(h)$, i.e. the cut singularity of $\mathcal{H}_H(h)$, with counterclockwise orientation in the complex h -plane. Note that (3.6) is the large- N limit of a set of weights of size $N/3$ and it follows from the identity [4]

$$\text{tr } \bar{A}^q = \sum_{k=1}^{N/3} \frac{\chi_{\{\tilde{h}_k^{(0)}(q)/3\}}(\bar{A})}{\chi_{\{h^{(0)}/3\}}(\bar{A})} \quad (3.7)$$

where

$$(\tilde{h}_k^{(0)}(q))_i = h_i^{(0)} + 3q\delta_{ik} \quad (3.8)$$

In the next section we shall discuss the evaluation of $\mathcal{F}(h)$ and the corresponding structure of the curvature matrix model as the vertex weights \tilde{t}_q^* are varied. Notice that, strictly speaking, in most cases of interest the characters corresponding to a specific choice of vertex weightings cannot be represented via matrix traces as in (1.4) and need to be defined by an analytical continuation. This can be accomplished by using the Schur-Weyl duality theorem to represent the $GL(N, \mathbb{C})$ characters as the generalized Schur functions

$$\chi_{\{h\}}[t^*] = \det_{k,\ell} [P_{h_k+1-\ell}[t^*]] \quad (3.9)$$

where $P_n[t^*]$ are the Schur polynomials defined by

$$\exp \left(N \sum_{q=1}^{\infty} z^q t_q^* \right) = \sum_{n=0}^{\infty} z^n P_n[t^*] \quad (3.10)$$

When the weights t_q^* are given by (1.4), the Schur functions (3.9) coincide with the Weyl characters (2.3).

Our first observation here is that the saddle-point equation (3.3) is identical to that of the even-even coordination number model discussed in [4, 5] which is defined by replacing the

cubic interaction matrix potential $V_3(XA)$ in (1.1) by

$$V_{\text{even}}(XA) = \sum_{q=1}^{\infty} t_{2q} (XA^{(2)})^{2q} \quad (3.11)$$

where

$$A^{(2)} = \begin{pmatrix} \tilde{A}^{1/2} & 0 \\ 0 & -\tilde{A}^{1/2} \end{pmatrix} \quad (3.12)$$

with $\tilde{A}^{1/2}$ an invertible $\frac{N}{2} \times \frac{N}{2}$ Hermitian matrix, and

$$2qt_{2q} = 2qt_{2q}^* = 2 \frac{\text{tr}}{N} \tilde{A}^q \quad (3.13)$$

The curvature matrix model with potential (3.11) generates a sum over random surfaces where arbitrary even coordination number vertices of the primary and dual lattices are permitted and are weighted identically, so that the model (3.11) is self-dual. In fact, the same saddle-point equation arises from the interaction potential

$$V_4(XA) = \frac{1}{4} (XA^{(2)})^4 \quad (3.14)$$

The matrix model with potential V_4 generates discretizations built up from even-sided polygons with 4-point vertices.

As shown in [4], the Itzykson-Di Francesco formula for the curvature matrix model with potential (3.11) follows from replacing $\mathcal{X}_3[h]$ in (2.5) by

$$\chi_{\{h\}}(A^{(2)}) = \chi_{\left\{\frac{h^e}{2}\right\}}(\tilde{A}) \chi_{\left\{\frac{h^o-1}{2}\right\}}(\tilde{A}) \text{ sgn} \left[\prod_{i,j=1}^{N/2} (h_i^e - h_j^o) \right] \quad (3.15)$$

Now the even and odd weights can be naturally assumed to distribute equally, and the effective action is

$$S_{\text{even}}[h^e] = -\frac{1}{4} \log \lambda + \frac{2}{N^2} \sum_{i < j}^{N/2} \log(h_i^e - h_j^e) + \frac{1}{N} \sum_{i=1}^{N/2} h_i^e [\log(\lambda h_i^e) - 1] + 4 \log I \left[\frac{Nh^e}{2}, \tilde{A} \right] \quad (3.16)$$

Defining a distribution function for the $N/2$ weights h_i^e analogously to that above and varying the action (3.16) yields the saddle-point equation (3.3) with $\lambda^3 \rightarrow \lambda$. In this case the Itzykson-Zuber correlator $\mathcal{F}(h)$ is determined as in (3.6) but now with $q\tilde{t}_q^*$ defined to be equal to (3.13) (i.e. the large- N limit of a set of weights of size $N/2$).

Likewise, in the case of the 4-point model (3.14), we replace $\mathcal{X}_3[h]$ by

$$\mathcal{X}_4[h] = \left(\frac{N}{4} \right)^{\frac{1}{4} \sum_i h_i} \prod_{\mu=0}^3 \frac{\Delta[h^{(\mu)}]}{\prod_{i=1}^{N/4} \left(\frac{h_i^{(\mu)} - \mu}{4} \right)!} \text{ sgn} \left[\prod_{0 \leq \mu_1 < \mu_2 \leq 3} \prod_{i,j=1}^{N/4} (h_i^{(\mu_2)} - h_j^{(\mu_1)}) \right] \quad (3.17)$$

where now the character sum is supported on weights that factor equally into their congruence classes $h_i^{(\mu)}$, $\mu = 0, \dots, 4$, $i = 1, \dots, \frac{N}{4}$, modulo 4. Because of the original weight constraint of the Itzykson-Di Francesco formula, this means that the even weights h_i^e distribute equally into the mod 4 congruence classes $\mu = 0, 2$ and the odd weights h_i^o into the classes $\mu = 1, 3$. Again, assuming these weights all distribute equally leads to the effective action

$$S_4[h^e] = -\frac{1}{4} \log \lambda + \frac{1}{N^2} \sum_{i < j}^{N/2} \log(h_i^e - h_j^e) + \frac{1}{2N} \sum_{i=1}^{N/2} h_i^e [\log(\lambda^2 h_i^e) - 1] + 2 \log I \left[\frac{Nh^e}{2}, \tilde{A} \right] \quad (3.18)$$

Introducing a distribution function for the $N/2$ weights h_i^e again leads to precisely the same saddle-point equation (3.3) with $\lambda^3 \rightarrow \lambda^2$. Here and in the even-even model above, unlike the 3-point model of the previous section, the large- N configuration of weights naturally localizes onto h_i^e .

These three matrix models therefore all possess the same solution at $N = \infty$, i.e. their random surface ensembles of genus zero graphs are identical. Their $1/N$ corrections will differ somewhat because of the different ways that the weights split into the respective congruence classes in the three separate cases. The genus zero free energies are related in a simple fashion. From (2.11) and the definition of the Hermitian distribution function, the genus zero free energy for the 3-point model is

$$S_H[\lambda, \tilde{t}_q^*] = \frac{1}{6} \left(\frac{1}{2} \int_0^a \int_0^a dh dh' \rho_H(h) \rho_H(h') \log |h - h'| + \int_0^a dh \rho_H(h) h [\log(\lambda^3 h) - 1] \right. \\ \left. + 2 \int_0^a dh \rho_H(h) \log I_c[h, \tilde{A}] \right) - \frac{1}{4} \log \lambda \quad (3.19)$$

where $\rho_H(h)$ is the solution of the saddle-point equation (3.3) and $\log I_c[h, \tilde{A}] = 3^2 \log I[\frac{Nh^{(0)}}{3}, \tilde{A}]$ is the Itzykson-Zuber integral (2.12) at $N = \infty$. Similarly, the genus zero free energies for the even-even and 4-point models can be written using the same distribution function $\rho_H(h)$. Now, however, the rules for replacing sums by integrals differ. For the even-even and 4-point models the normalized sums corresponding to a spectral density normalized to unity are $\frac{2}{N} \sum_{i=1}^{N/2}$ and the $N = \infty$ Itzykson-Zuber integral is $\log I_c[h, \tilde{A}] = 2^2 \log I[\frac{Nh^e}{2}, \tilde{A}]$. Taking this into account along with the change of λ in the three cases, we find that the free energies of the three models discussed above are all related by

$$3S_H[\lambda^{2/3}, \tilde{t}_q^*] = 2S_4[\lambda, \tilde{t}_q^*] = S_{\text{even}}[\lambda^2, \tilde{t}_q^*] \quad (3.20)$$

It is quite intriguing that the Itzykson-Di Francesco formula naturally implies these relations by dictating the manner in which the Young tableau weights should decompose with respect to the appropriate congruence classes in each case. This is reflected in both the overall numerical coefficients and the overall powers of λ that appear in (3.20). In the next subsection we shall give purely graph-theoretical proofs of these relationships. This yields a non-trivial

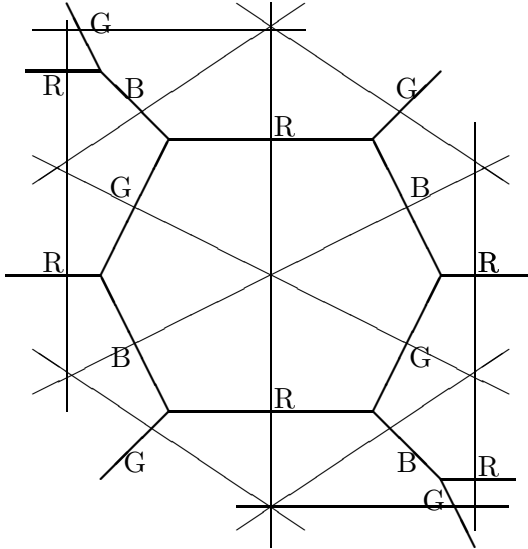


Figure 1: A 3-colouring of a graph in \mathcal{M}_3 (thick lines) and its associated dual graph in \mathcal{M}_3^* (thin lines).

verification of the assumptions made in section 2 about the splitting of the Young tableau weights for the dynamical triangulation model.

3.2 Graph Theoretical Relationships

Before pursuing further the properties of the curvature matrix model above, we present a direct, graphical proof of the relationship (3.20) between the generating functions for the 3-point, 4-point, and even-even planar graphs. We denote the ensembles of spherical graphs in these three cases by \mathcal{M}_3 , \mathcal{M}_4 and $\mathcal{M}_{\text{even}}$, respectively. We first discuss the mapping $\mathcal{M}_3 \rightarrow \mathcal{M}_4$. Consider a planar graph $G \in \mathcal{M}_3$. Using a version of the colouring theorem for a spherical topology, we can colour the lines of G by three colours, R, B, and G, to give a planar graph G^c with labelled lines (Fig. 1). Because G consists of polygons whose numbers of sides are all multiples of three, the colouring can be chosen so that the three colours always occur in the sequence (R,B,G) as one goes around any polygon of G^c with clockwise orientation. We can now contract the two 3-point vertices bounding each R-link of G^c into a 4-point vertex (Fig. 2). A polygon of $3m$ sides with 3-point vertices in G^c then becomes a polygon of $2m$ sides with 4-point vertices. The resulting 2-coloured graph \tilde{G}^c thus belongs to \mathcal{M}_4 . Notice that if each link has a weight λ associated to it, then the effect of the R-contractions is to map $\lambda^3 \rightarrow \lambda^2$ on $\mathcal{M}_3 \rightarrow \mathcal{M}_4$.

Conversely, suppose $\tilde{G} \in \mathcal{M}_4$. We can form a 2-coloured graph \tilde{G}^c , with colours B and G,

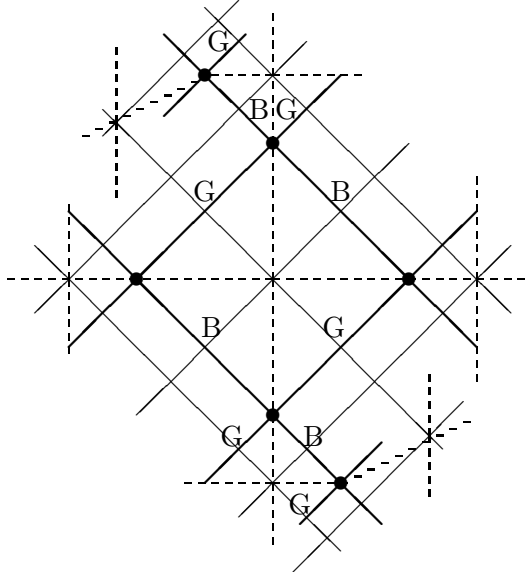


Figure 2: A 2-colouring of a graph in \mathcal{M}_4 (thick lines), its associated dual graph in \mathcal{M}_4^* (thin lines), and the corresponding diagram in $\mathcal{M}_{\text{even}}$ (dashed lines). The 4-point vertices denoted by solid circles are contracted from the R-links of the corresponding graph of \mathcal{M}_3 depicted in Fig. 1.

such that the colours alternate along the lines of \tilde{G}^c (Fig. 2). There are two possible ways to orient lines of \tilde{G}^c , by defining a direction to them from either B to G or from G to B at each vertex. The 4-point vertices of the resulting oriented graph can then be split into a line, labelled by R, bounded by two 3-point vertices. There are two ways of doing this, by splitting the 4-point vertex either vertically or horizontally with respect to the given orientation (Fig. 3). Thus to each 2-coloured graph $\tilde{G}^c \in \mathcal{M}_4$ there corresponds two distinct (topologically inequivalent) 3-coloured graphs $G^c \in \mathcal{M}_3$. There are also three distinct 2-coloured graphs $\tilde{G}^c \in \mathcal{M}_4$ for each 3-coloured graph $G^c \in \mathcal{M}_3$ corresponding to the three possible choices of contraction colour R, B or G. This therefore defines a three-to-two mapping on $\mathcal{M}_4 \rightarrow \mathcal{M}_3$ and is just the statement of the first equality of (3.20).

Actually, there exists a simpler, line mapping between these two ensembles of graphs in terms of dual lattices. Let \mathcal{M}_3^* denote the collection of planar graphs dual to those of \mathcal{M}_3 (i.e. lattices built up from triangles that form $3m$ -valence vertices), and \mathcal{M}_4^* the dual ensemble to \mathcal{M}_4 (i.e. the graphs formed of squares that meet to form vertices of even coordination number). The sets \mathcal{M}_3^* and \mathcal{M}_4^* are generated, respectively, by the curvature matrix models with matrix potentials

$$V_3^{(*)}(XA) = \sum_{q=1}^{\infty} t_{3q}^*(XA_3)^{3q} \quad , \quad V_4^{(*)}(XA) = \sum_{q=1}^{\infty} t_{2q}(XA_4)^{2q} \quad (3.21)$$

where the $N \times N$ matrix A_m is defined by $\frac{\text{tr}}{N} A_m^k = \delta_m^k$. The corresponding generating functions $S_H^{(*)}[\lambda, \tilde{t}_q^*]$ and $S_4^{(*)}[\lambda, \tilde{t}_q^*]$ coincide, respectively, with (2.11) and (3.18) [4]. Again the lines of

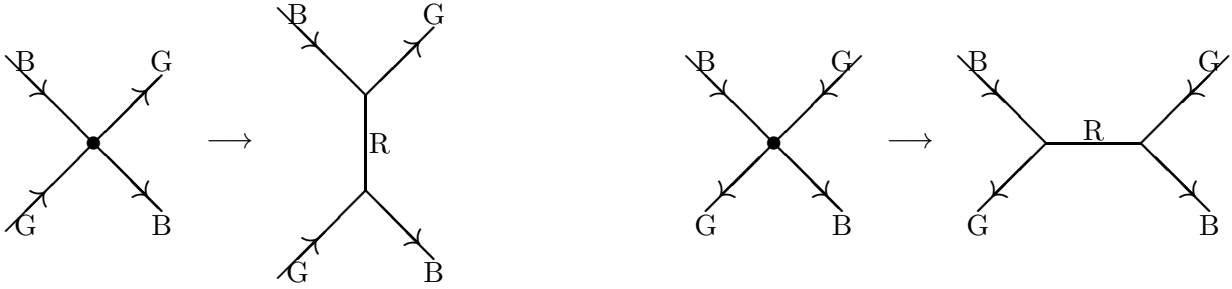


Figure 3: The two possible 4-point vertex splittings which respect the given B and G colour orientation.

the graphs of \mathcal{M}_3^* can be 3-coloured, and the deletion of all R-coloured lines gives a map $\mathcal{M}_3^* \rightarrow \mathcal{M}_4^*$ (Figs. 1 and 2). This mapping is three-to-one because of the three possible choices of deletion colour. The inverse map $\mathcal{M}_4^* \rightarrow \mathcal{M}_3^*$, defined by inserting an R-link across the diagonal of each square of the graphs of \mathcal{M}_4^* , is then two-to-one because of the two possible choices of diagonal of a square.

The correspondence between the ensembles of graphs \mathcal{M}_4 and $\mathcal{M}_{\text{even}}$ is similar and has been noted in [5] (see Fig. 2). Given a graph $G^* \in \mathcal{M}_4^*$, we choose a diagonal of each square of G^* . Connecting these diagonals together produces a graph in $\mathcal{M}_{\text{even}}$. Equivalently, we can place vertices in the face centers of the corresponding dual graph $G \in \mathcal{M}_4$ and connect them together by drawing lines through each of the 4-point vertices of G (so that $\lambda^4 \rightarrow \lambda^8$ from the splitting of these 4-point vertices). In this way we obtain a map $\mathcal{M}_4, \mathcal{M}_4^* \rightarrow \mathcal{M}_{\text{even}}$ where the vertices and face centers of graphs of $\mathcal{M}_{\text{even}}$ correspond to the vertices of graphs of \mathcal{M}_4^* , or equivalently the faces of \mathcal{M}_4 . Because there are two distinct ways of choosing the diagonal of a square of $G^* \in \mathcal{M}_4^*$ (equivalently two ways of splitting a 4-point vertex of $G \in \mathcal{M}_4$ with respect to a 2-colour orientation analogously to that in Fig. 3), this mapping is two-to-one and corresponds to the second equality of (3.20). In particular, there is a three-to-one correspondence between graphs of $\mathcal{M}_3, \mathcal{M}_3^*$ and $\mathcal{M}_{\text{even}}$.

We stress that these graphical mappings are only valid on the sphere. In terms of the Itzykson-Di Francesco formula, this means that the $\mathcal{O}(1/N)$ corrections to the large- N saddle-point solutions of the corresponding curvature matrix models will differ. These non-trivial correspondences are predicted from the matrix model formulations, because in all cases we obtain the same $N = \infty$ saddle-point equations but different splittings of Young tableau weights into congruence classes thus leading to different overall combinatorical factors in front of the graph generating function. Note that in the case of the 4-point and even-even models the vertex weights \tilde{t}_q^* are mapped into each other under the above graphical correspondence because of the simple line map that exists between $\mathcal{M}_{\text{even}}$ and \mathcal{M}_4^* . In the case of the mappings

onto \mathcal{M}_3 the weights \tilde{t}_q^* defined in (3.6) are mapped onto those defined by (3.13) because of the contraction of $3m$ -sided polygons into $2m$ -sided polygons.

3.3 Complex Model

As mentioned in section 2, it is useful to compare the Hermitian 3-point curvature matrix model with the complex one since in the latter case the Young tableau weights completely factorize and the splitting of them into mod 3 congruence classes appears symmetrically. The saddle-point solution in the case of the complex curvature matrix model is identical in most respects to that of the Hermitian models above. Now the spectral density $\rho_C(h)$ for the Young tableau weights $h_i^{(0)}$, $i = 1, \dots, \frac{N}{3}$, obeys the saddle-point equation

$$\int_b^a dh' \frac{\rho_C(h')}{h - h'} = -\log(\lambda^{3/2}h) - \log\left(\frac{h}{h - b}\right) - \frac{1}{2}\mathcal{F}(h) \quad , \quad h \in [b, a] \quad (3.22)$$

where the logarithmic derivative $\mathcal{F}(h)$ of the Itzykson-Zuber integral is defined just as in (3.2). The solution for $\mathcal{F}(h) = 0$ is thus identical to those above. In particular, working out the free energy as before we see that

$$S_C[\lambda, \tilde{t}_q^*] = 4S_H[\rho_C; \sqrt{\lambda}, \tilde{t}_q^*] - \int_0^a dh \rho_C(h) \log I_c[h, \bar{A}] \quad (3.23)$$

The combinatorial factors appearing in (3.23) can be understood from the Wick expansions of the Hermitian and complex curvature matrix models. First consider the case $\mathcal{F}(h) = 0$. One factor of 2 appears in front of S_H in (3.23) because the number of independent degrees of freedom of the $N \times N$ complex matrix model is twice that of the $N \times N$ Hermitian curvature matrix model. The other factor of 2 arises from the mapping of Feynman graphs of the complex matrix model onto those of the Hermitian model (Fig. 4). At each 6-point vertex of a complex graph we can place a ϕ^\dagger line beside a ϕ line to give a graph with 3-point vertices and “thick” lines (each thick line associated with a $\phi^\dagger\phi$ pair of lines). This maps the propagator weights as $\lambda^6 \rightarrow \lambda^3$ and there are $3!/3 = 2$ distinct ways of producing a complex graph by thickening and splitting the lines of a graph in \mathcal{M}_3 in this way. This is the relation (3.23) for $I_c \equiv 1$. In the general case, there is a relative factor of 4 in front of the Itzykson-Zuber correlator in (3.22) because the Feynman rules for the complex curvature matrix model associate the weights

$$t_q^{C*} = \frac{1}{q} \frac{\text{tr}}{N} \left(A^{1/2} \right)^q \quad (3.24)$$

to the dual vertices v_q^* of the Feynman graphs (compare with (1.4)). Thus for $q\tilde{t}_q^* \neq 1$, the free energy of the complex model differs from (3.19) in a factor of 4 in front of the integral involving the Itzykson-Zuber integral $I_c[h, \bar{A}]$.

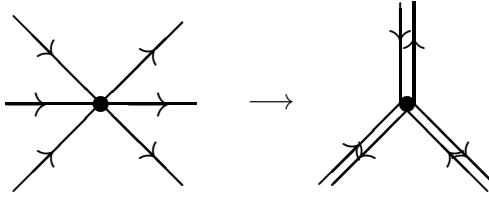


Figure 4: The mapping of a complex model 6-point vertex onto a Hermitian model 3-point vertex. The incoming lines represent the ϕ^\dagger fields, the outgoing lines the ϕ fields, and the solid circle denotes an insertion of the matrix $A^{1/2}$.

The complex curvature matrix model with the above rules thus generates “checkered” Riemann surfaces corresponding to the double-lined triangulations shown in Fig. 4. A 3-colouring of a graph of \mathcal{M}_3 is now described by a sort of 6-colouring whereby each colour R, B, and G is assigned an incoming and outgoing orientation at each vertex. Again these relations are only valid at $N = \infty$. However, the models lie in the same universality class (as with the even coordination number models discussed above) and consequently their double scaling limits will be the same. In particular, the equivalences (3.20) and (3.23) will hold to all genera near the critical point [14] (see the next subsection).

3.4 Critical Behaviour and Correlation Functions

We will now discuss to what extent the above models are universal. First, let us find the explicit solution of the saddle-point equation (3.3) in the case $\mathcal{F}(h) = 0$ [4] (i.e. $\bar{A} = \tilde{A} = \mathbf{1}$ and $q\tilde{t}_q^* = 1$). Notice that in this case the dual potentials in (3.11) and (3.21) become the Penner-type potentials [3, 9]

$$\begin{aligned} V_{\text{even}}(XA) &= -\frac{1}{2} \log \left(\mathbf{1} - (XA^{(2)})^2 \right) \quad , \quad V_4^{(*)}(XA) = -\frac{1}{2} \log \left(\mathbf{1} - (XA_4)^2 \right) \\ V_3^{(*)}(XA) &= -\frac{1}{3} \log \left(\mathbf{1} - (XA_3)^3 \right) \end{aligned} \quad (3.25)$$

so that the above arguments imply the equivalences between the curvature matrix model for a dynamical triangulation and those of Penner models. The behaviour of the saddle-point solution when the dual vertices v_q^* are not weighted equally will be examined in the next section.

The saddle-point equation (3.3) determines the continuous part of the resolvent function $\mathcal{H}_H(h)$ across its cut. Using the normalization $\int_0^a dh \rho_H(h) = 1$ of the spectral density in (3.4) implies the asymptotic boundary condition $\mathcal{H}_H(h) \sim 1/h$ at $|h| \rightarrow \infty$. It follows that

the solution for the resolvent function is given by [1]

$$\begin{aligned}\mathcal{H}_H(h) &= \log\left(\frac{h}{h-b}\right) - \oint_{\mathcal{C}} \frac{ds}{2\pi i} \frac{1}{s-h} \sqrt{\frac{(h-a)(h-b)}{(s-a)(s-b)}} \int_b^a dh' \frac{\rho_H(h')}{s-h'} \\ &= \log\left(\frac{h}{h-b}\right) + \oint_{\mathcal{C}} \frac{ds}{2\pi i} \frac{1}{s-h} \sqrt{\frac{(h-a)(h-b)}{(s-a)(s-b)}} \left\{ \log(\lambda^3 s) + \log\left(\frac{s}{s-b}\right) \right\}\end{aligned}\quad (3.26)$$

The contour integrations in (3.26) can be evaluated by blowing up the contour \mathcal{C} to infinity and catching the contributions from the cuts of the two logarithms, on $(-\infty, 0]$ and $[0, b]$, respectively, and also from the simple pole at $s = h$. Keeping careful track of the signs of the square roots on each cut and taking discontinuities across these cuts, after some algebra we arrive at

$$\begin{aligned}\mathcal{H}_H(h) &= -\log(\lambda^3 h) + \sqrt{(h-a)(h-b)} \left\{ \int_0^b - \int_{-\infty}^0 \right\} \frac{dx}{x-h} \frac{1}{\sqrt{(x-a)(x-b)}} \\ &= \log \left\{ \frac{a-b}{\lambda^3(\sqrt{a} + \sqrt{b})^2} \frac{(h + \sqrt{ab} + \sqrt{(h-a)(h-b)})^2}{h(h(a+b) - 2ab + 2\sqrt{ab(h-a)(h-b)})} \right\}\end{aligned}\quad (3.27)$$

It remains to solve for the endpoints a, b of the support of the spectral distribution function in terms of the parameters of the matrix potential. They are determined by expanding the function (3.27) for large- h , and requiring that the constant term vanish and that the coefficient of the $1/h$ term be 1. This leads to a pair of equations for a, b

$$\xi = \frac{1}{3}(\eta - 1) \quad , \quad 3\lambda^6\eta^3 = \eta - 1 \quad (3.28)$$

where we have introduced the positive endpoint parameters

$$\xi = \frac{1}{4}(\sqrt{a} - \sqrt{b})^2 \quad , \quad \eta = \frac{1}{4}(\sqrt{a} + \sqrt{b})^2 \quad (3.29)$$

The cubic equation for η in (3.28) can be solved explicitly. The original matrix model free energy is analytic around $\lambda = 0$. We shall see below that it is analytic in η , so that we should choose the branch of the cubic equation in (3.28) which is regular at $\lambda = 0$. This solution is found to be

$$\eta = -\frac{1}{2}\beta^{1/3} - \frac{1}{18\lambda^6\beta^{1/3}} - i\sqrt{3} \left(\beta^{1/3} - \frac{1}{9\lambda^6\beta^{1/3}} \right) \quad (3.30)$$

where

$$\beta = -\frac{1}{6\lambda^6} + \frac{1}{54\lambda^9} \sqrt{81\lambda^6 - 4} \quad (3.31)$$

The solution (3.30) leads to the appropriate boundary condition $\eta(\lambda = 0) = 1, \xi(\lambda = 0) = 0$, i.e. $a = b = 1$, as expected since in this case the spectral density should be trivial, $\rho_H(h) \equiv 1$.

The solution (3.30) is real-valued for $\lambda < \lambda_c \equiv (2/9)^{1/3}$ which is the regime wherein all three roots of the cubic equation for η in (3.28) are real. For $\lambda > \lambda_c$ there is a unique real-valued solution which does not connect continuously with the real solution that is regular at $\lambda = 0$. At $\lambda = \lambda_c$ the pair of complex-conjugate roots for $\lambda > \lambda_c$ coalesce and become real-valued. Thus for $\lambda > \lambda_c$ the one-cut solution above for \mathcal{H}_H is no longer valid and the spectral density ρ_H becomes supported on more than one interval. The value $\lambda = \lambda_c$ is therefore identified as the critical point of a phase transition of the random surface theory which corresponds to a change of analytic structure of the saddle-point solution of the matrix model. As usual, at this critical point the continuum limit of the discretized random surface model, describing the physical string theory, is reached. To determine the precise nature of the geometry that is obtained in this continuum limit, we need to study the scaling behaviour of the matrix model free energy near the critical point. In the following we shall present two calculations illustrating this critical behaviour.

3.4.1 Propagator

As shown in [4, 5], in the general case the resolvent function $\mathcal{H}_H(h)$ and the Itzykson-Zuber correlator $\mathcal{F}(h)$ completely determine the solution of the random matrix model in the large- N limit. For instance, expectation values of the operators $\frac{\text{tr}}{N}X^{2q}$ can be obtained from the contour integral

$$\left\langle \frac{\text{tr}}{N}X^{2q} \right\rangle_{\mathcal{M}_3} = \frac{\lambda^q}{q} \oint_C \frac{dh}{2\pi i} h^q e^{q\mathcal{H}_H(h)} \quad (3.32)$$

where the normalized average is with respect to the partition function (1.1) and the decomposition (2.6). The expression (3.32) holds only for the even moments of the matrix X because it is only for such moments that the character expansion of the right-hand side of (3.32) admits a symmetrical even-odd decomposition as in the Itzykson-Di Francesco formula [4]. Although a character expansion for the odd moments can be similarly derived, the weights will not split symmetrically and there does not appear to be a general expression for them in terms of the weight distribution function at large- N . For the even coordination number models above, the reflection symmetry $X \rightarrow -X$ of the matrix model forces the vanishing of all odd moments automatically and (3.32) represents the general expression for the complete set of observables which do not involve the external field A at large- N . In terms of the character expansion formula, the character sum for $\langle \frac{\text{tr}}{N}X^{2q+1} \rangle$ vanishes in the case of an even potential because of the localization onto the even representations of $GL(N, \mathbb{C})$, whereas in the 3-point model $\langle \frac{\text{tr}}{N}X^{2q+1} \rangle_{\mathcal{M}_3} \neq 0$ because its character sum is supported on mod 3 congruence class representations.

The contour integral representation (3.32), with \mathcal{H}_H replaced by \mathcal{H}_C , also holds for the correlators $\langle \frac{\text{tr}}{N}(\phi^\dagger\phi)^q \rangle_C$ of the complex curvature matrix model. These averages form the

complete set of A -independent observables at large- N in this case because of the charge conjugation symmetry $\phi \rightarrow \phi^\dagger$ of the complex model (which is the analogue here of the reflection symmetry of the even coordination number models). Again this indicates that the complex curvature matrix model is better suited to represent the triangulated random surface sum, because it is more amenable to an explicit solution in the large- N limit. Furthermore, its complete set of correlation functions coincide at $N = \infty$ with those of the equivalent matrix models defined above with even potentials, after redefining the vertex weights according to (1.4) and (3.24).

The contour integral on the right-hand side of (3.32) can be evaluated by blowing up the contour \mathcal{C} , expanding the resolvent function (3.27) for large- h , and computing the residue at $h = \infty$. For example, for $q = 1$ we have

$$\left\langle \frac{\text{tr}}{N} X^2 \right\rangle_{\mathcal{M}_3} = \lambda \left(\frac{1}{2} + \langle h \rangle \right) \quad (3.33)$$

where the weight average $\langle h \rangle = \langle \frac{3}{N} \sum_{i=1}^{N/3} h_i^{(0)} \rangle = \int_0^a dh \rho_H(h)h$ corresponds to the coefficient of the $1/h^2$ term in the asymptotic expansion of (3.27). This result also follows directly from differentiating the free energies

$$\left\langle \frac{\text{tr}}{N} X^2 \right\rangle = 2\lambda^2 \frac{\partial}{\partial \lambda} S[\lambda, t_q^*] \quad , \quad \left\langle \frac{\text{tr}}{N} \phi^\dagger \phi \right\rangle_C = \lambda^2 \frac{\partial}{\partial \lambda} S_C[\lambda, t_q^*] \quad (3.34)$$

and using the saddle-point equations. Notice that (3.34) and the free energy relations (3.20) and (3.23) imply, in particular, that the matrix propagators of the 3-point, 4-point, even-even and complex matrix models coincide with the appropriate redefinitions of the coupling constants λ and t_q^* . However, the equivalences of generic observables in the various models will not necessarily hold. We shall return to this point shortly.

Using (3.27) and (3.28), the propagator (3.33) can be written as

$$\left\langle \frac{\text{tr}}{N} X^2 \right\rangle_{\mathcal{M}_3} = \lambda \left(\frac{1}{3} - \frac{\eta^2}{3} + \eta \right) \quad (3.35)$$

Expanding (3.35) using (3.30) as a power series in λ yields

$$\left\langle \frac{\text{tr}}{N} X^2 \right\rangle_{\mathcal{M}_3} = \lambda + \lambda^7 + 6\lambda^{13} + 54\lambda^{19} + 594\lambda^{25} + \mathcal{O}(\lambda^{31}) \quad (3.36)$$

We have verified, by an explicit Wick expansion of the matrix propagator (up to and including the order shown in (3.36)) using the $3m$ -sided polygon constraints on the matrix traces (1.4), that (3.36) indeed coincides with perturbative expansion of the curvature matrix model (1.1) and thus correctly counts the planar 3-point fat graphs consisting of only $3m$ -sided polygons. It also agrees with the Wick expansions of the even coordination number models above [4] and of the complex curvature matrix model.

To examine the scaling behaviour of observables of the matrix model near the critical point, we introduce a renormalized, continuum cosmological constant Λ and momentum Π by

$$\lambda^6 = \lambda_c^6(1 - \Lambda) \quad , \quad \eta = \eta_c - \Pi/2 \quad (3.37)$$

where $\eta_c = \eta(\lambda = \lambda_c) = 3/2$. We then approach the critical point along the line $\Lambda, \Pi(\Lambda) \rightarrow 0$, where the function $\Pi(\Lambda)$ is found by substituting the definitions (3.37) into (3.30) to get

$$\Pi(\Lambda) = -\frac{1}{2} \left[\Xi^{1/3} + \frac{9(\Lambda_* + 1)}{\Xi^{1/3}} - 6 + i\sqrt{3} \left(\Xi^{1/3} - \frac{9(\Lambda_* + 1)}{\Xi^{1/3}} \right) \right] \quad (3.38)$$

with

$$\Xi = 27 \left(\Lambda_* + 1 + \sqrt{-\Lambda_*^3 - 2\Lambda_*^2 - \Lambda_*} \right) \quad , \quad \Lambda_* = \frac{\Lambda}{1 - \Lambda} \quad (3.39)$$

Substituting (3.37) and (3.38) into (3.35) and expanding around $\Lambda = 0$ yields after some algebra

$$\left\langle \frac{\text{tr}}{N} X^2 \right\rangle_{\mathcal{M}_3} = \frac{2}{9} \Lambda^{3/2} + \dots \equiv c \cdot \Lambda^{1-\gamma_{\text{str}}} + \dots \quad (3.40)$$

where the dots denote terms which are less singular as $\Lambda \rightarrow 0$. The leading non-analytic behaviour in (3.40) identifies the critical string exponent of this random surface model as

$$\gamma_{\text{str}} = -1/2 \quad (3.41)$$

so that the system in the continuum limit represents pure two-dimensional quantum gravity [1]. The same argument also applies to the 4-point and even-even models with the appropriate redefinitions of cosmological constants in (3.37). Thus the equal weighting of all vertices in these random surface models leads to curvature matrix models in the same universality class as the more conventional Hermitian one-matrix models of two-dimensional quantum gravity. This agrees with recent numerical results in [15].

3.4.2 General Correlators

We now turn to a more general discussion of the evaluation of observables in the matrix models above. The relations between correlators involving the external matrix A are a bit more subtle than those represented by the contour integrations in (3.32) which coincide in all four matrix models for all q . Because of the simple line maps that exist between the ensembles \mathcal{M}_3^* , \mathcal{M}_4^* and $\mathcal{M}_{\text{even}}$, all expectation values are the same in these models, i.e.

$$\frac{1}{4} \left\langle \frac{\text{tr}}{N} (\phi^\dagger \phi A_3)^{3q} \right\rangle_{C^*} = \left\langle \frac{\text{tr}}{N} (X A_3)^{3q} \right\rangle_{\mathcal{M}_3^*} = \left\langle \frac{\text{tr}}{N} (X A_4)^{2q} \right\rangle_{\mathcal{M}_4^*} = \left\langle \frac{\text{tr}}{N} (X A^{(2)})^{2q} \right\rangle_{\mathcal{M}_{\text{even}}} \quad (3.42)$$

Analytically, this equality follows from the fact that these correlators are given by derivatives of the free energies of the matrix models with respect to the weights \tilde{t}_q^* . The powers in (3.42)

can be understood from the fact that the reflection symmetry $A^{(2)} \rightarrow -A^{(2)}$ of the \mathcal{M}_4 and $\mathcal{M}_{\text{even}}$ models (which restrict the non-zero averages to $\langle \frac{\text{tr}}{N} (XA^{(2)})^{2q} \rangle_{\mathcal{M}_4, \mathcal{M}_{\text{even}}}$) corresponds to the \mathbb{Z}_3 -symmetry $A^{(3)} \rightarrow \omega_3 A^{(3)}$, $\omega_3 \in \mathbb{Z}_3$, of the \mathcal{M}_3 model (which restricts the non-vanishing observables to $\langle \frac{\text{tr}}{N} (XA^{(3)})^{3q} \rangle_{\mathcal{M}_3}$ and $\langle \frac{\text{tr}}{N} (\phi^\dagger \phi A^{(3)})^{3q} \rangle_C$). In terms of the coloured graphs of subsection 3.2, these discrete symmetries correspond to permutations of the colours of graphs in each ensemble. It is these symmetries that are ultimately responsible for the localization of the Itzykson-Di Francesco character sum onto the appropriate even or mod 3 representations in each case.

The correlators in (3.42) are also given by a simple contour integration. It can be shown that [5]

$$\frac{1}{N} \frac{\partial}{\partial \tilde{t}_q^*} \log \chi_{\left\{ \frac{h^{(0)}}{3} \right\}}(\bar{A}) = \sum_{k=1}^{N/3} \frac{\chi_{\left\{ \tilde{h}_k^{(0)}(-q)/3 \right\}}(\bar{A})}{\chi_{\left\{ h^{(0)}/3 \right\}}(\bar{A})} \quad (3.43)$$

where $\tilde{h}_k^{(0)}$ is defined in (3.8). From the character expansion of section 2 we see that the left-hand side of (3.43) arises from a derivative of the dual model free energy $S_H^{(*)}[\lambda, \tilde{t}_q^*]$ with respect to the vertex weights \tilde{t}_q^* , whereas the right-hand side is identical to (3.7) with $q \rightarrow -q$. In the large- N limit, we can therefore represent the dual model correlators in (3.42) by the contour integrations

$$\left\langle \frac{\text{tr}}{N} (XA_3)^{3q} \right\rangle_{\mathcal{M}_3^*} = -\frac{\lambda^q}{q} \oint_{\mathcal{C}} \frac{dh}{2\pi i} e^{-q(\mathcal{H}_H(h) + \mathcal{F}(h))} \quad (3.44)$$

Although it is possible to determine the complete set of observables of the dual matrix models in terms of the saddle-point solution at large- N , the situation is somewhat more complicated for the correlators of the \mathcal{M}_3 and \mathcal{M}_4 ensembles. The above discussion illustrates to what extent the large- N saddle-point solution of the Itzykson-Di Francesco formula can be used to represent the observables of the matrix model. Those which do admit such a representation typically appear to be obtainable from derivatives of the free energy of the model and thus correspond in the random surface interpretation to insertions of marked loops on the surfaces. Thus, strictly speaking, the natural observable to compute in the large- N limit of the 3-point matrix model is the free energy (3.19). In the next subsection we shall show how this calculation carries through.

3.4.3 Free Energy

The natural observable to compute in the triangulation model is the large- N (genus zero) free energy (3.19) with $I_c = 1$. Splitting up the integration range and setting $\rho_H(h) = 1$ on $[0, b]$,

we find

$$S_H = \frac{1}{3} \int_b^a dh \rho_H(h)h \left[\log(\lambda^3 h) - 1 \right] + \frac{1}{3} \int_b^a dh \rho_H(h) [h \log h - (h-b) \log(h-b) - b] \\ + \frac{1}{6} \int_b^a \int_b^a dh dh' \rho_H(h) \rho_H(h') \log |h-h'| + \frac{b^2}{6} \left(\log b - \frac{3}{2} \right) + \frac{b^2 - 3/2}{4} \log \lambda \quad (3.45)$$

The spectral density is found by computing the discontinuity (3.5) of the weight resolvent function (3.27) across the cut $[b, a]$, which yields

$$\rho_H(h) = \frac{1}{\pi} \left[\arctan \left(\frac{2\sqrt{ab(a-h)(h-b)}}{(a+b)h - 2ab} \right) - 2 \arctan \left(\frac{\sqrt{(a-h)(h-b)}}{h + \sqrt{ab}} \right) \right] \quad , \quad h \in [b, a] \quad (3.46)$$

The double integral in the free energy (3.45) can be simplified by integrating up the saddle-point equation (3.3) for $h \in [b, a]$ to get

$$\int_b^a dh' \rho_H(h') \log |h-h'| = h \left[1 - \log(\lambda^3 h) \right] + (h-b) \log(h-b) - h \log h + \frac{1}{4} \log \lambda \\ + \int_b^a dh' \rho_H(h') \log(h'-b) + b \left[\log(\lambda^3 b) - 1 \right] + b \log b \quad (3.47)$$

Substituting (3.47) into (3.45) and integrating by parts, we find after some algebra

$$S_H = -\frac{1}{6} \int_b^a dh \frac{d\rho_H(h)}{dh} \left\{ h \left[h \log h - \frac{h}{2} \log(h-b) + \log(h-b) \right] - b \left(1 - \frac{b}{2} \right) \log(h-b) \right\} \\ + \frac{b}{3} \log b \left(1 - \frac{b}{2} \right) + \frac{b}{6} \log \lambda - \frac{b}{12} (b+15) + \frac{\langle \tilde{h} \rangle}{6} \left(\log \lambda - \frac{3}{2} \right) \quad (3.48)$$

where we have introduced the reduced weight average $\langle \tilde{h} \rangle = \int_b^a dh \rho_H(h)h = \langle h \rangle - b^2/2$, and from (3.46) we have

$$\frac{d\rho_H(h)}{dh} = \frac{h - 2\sqrt{ab}}{\pi \sqrt{(a-h)(h-b)}} \quad , \quad h \in [b, a] \quad (3.49)$$

The weight average $\langle h \rangle$ can be read off from (3.27) to give

$$\langle h \rangle = -\eta^2/3 + \eta - 1/6 \quad (3.50)$$

To evaluate the remaining logarithmic integrals in (3.48), it is convenient to change variables from $h \in [b, a]$ to $x \in [-1, 1]$ with $h = \frac{1}{2}(a+b) + \frac{1}{2}(a-b)x$. This leads to a series of integrals over elementary algebraic forms and forms involving logarithmic functions. The latter integrals can be computed by rewriting the integrations over $x \in [-1, 1]$ as contour integrals, blowing up the contours and then picking up the contributions from the discontinuities

across the cuts of the logarithms. The relevant integrals are then found to be

$$\begin{aligned}
I_0(r) &= \int_{-1}^1 dx \frac{\log(1+rx)}{\sqrt{1-x^2}} = \pi \log\left(\frac{1+\sqrt{1-r^2}}{2}\right) \\
I_1(r) &= \int_{-1}^1 dx \frac{x \log(1+rx)}{\sqrt{1-x^2}} = \frac{\pi}{r} \left(1 - \sqrt{1-r^2}\right) \\
I_2(r) &= \int_{-1}^1 dx \frac{x^2 \log(1+rx)}{\sqrt{1-x^2}} = \frac{1}{2} \left(I_0(r) - \frac{I_1(r)}{r} + \frac{\pi}{2}\right) \\
J(r) &= \int_{-1}^1 dx \frac{\log(1+x)}{(1+rx)\sqrt{1-x^2}} = -\pi \int_{-\infty}^{-1} \frac{dy}{(1+ry)\sqrt{1-y^2}} + \frac{\pi \log\left(\frac{1-r}{r}\right)}{\sqrt{1-r^2}} \\
&= \frac{\pi}{\sqrt{1-r^2}} \log\left(\frac{1-r}{1+\sqrt{1-r^2}}\right)
\end{aligned} \tag{3.51}$$

where $0 \leq r \leq 1$. Using the above identities and the boundary conditions (3.28), after some tedious algebra we arrive finally at the simple expression

$$S_H(\eta) = \frac{1}{4} \log \lambda + \frac{1}{6} \log \eta + \frac{\eta^2}{36} - \frac{7\eta}{36} \tag{3.52}$$

for the free energy of the triangulation model, where we have ignored an overall numerical constant.

To examine the scaling behaviour of the free energy about the critical point, we once again introduce a renormalized, continuum cosmological constant Λ and momentum Π as in (3.37). From the boundary equation $3\lambda^6\eta^3 = \eta - 1$ we can calculate derivatives of η with respect to the cosmological constant to get

$$\frac{\partial \eta}{\partial \Lambda} = -\frac{3\lambda_c^6 \eta^4}{\eta - \eta_c} \tag{3.53}$$

which we note diverges at the critical point. From (3.52) and (3.53) the first two derivatives of the free energy are then found to be

$$\frac{\partial S_H}{\partial \Lambda} = -\lambda_c^6 \eta^3 (\eta - 2)/6 \quad , \quad \frac{\partial^2 S_H}{\partial \Lambda^2} = 2\lambda_c^{12} \eta^6 \tag{3.54}$$

Both derivatives in (3.54) are finite at the critical point. Taking one more derivative yields a combination that does not cancel the singular $(\eta - \eta_c)^{-1}$ part of (3.53), i.e. there is a third order phase transition at the critical point. Substituting (3.37) into the boundary equation (3.28) gives $\Pi^2 \sim \Lambda$ near criticality $\Lambda \rightarrow 0$ (see (3.38), (3.39)), and so substituting $\eta \sim \eta_c - \Lambda^{1/2}$ into (3.54) and expanding about $\Lambda = 0$ yields

$$\frac{\partial^2 S_H}{\partial \Lambda^2} = c \cdot \Lambda^{1/2} + \dots \tag{3.55}$$

which identifies the expected pure gravity string exponent (3.41).

4 Incorporation of the Itzykson-Zuber Correlator

In this section we shall give a more quantitative presentation of the evaluation of observables in the curvature matrix models and how they reproduce features of the triangulated random surface sum. This will also further demonstrate the validity of the weight splitting that was assumed to hold in the Itzykson-Di Francesco formula, i.e. that the leading order contributions to the partition function indeed do localize at $N = \infty$ onto the even representations of $GL(N, \mathbb{C})$ that split symmetrically into mod 3 congruence classes. For this we shall present an explicit evaluation of the Itzykson-Zuber correlator $\mathcal{F}(h)$ using (3.6). This will amount to an evaluation of the large- N limit of the generalized Schur functions introduced in the previous section.

Notice first that expanding both sides of (3.6) in powers of q and equating the constant terms leads to the identity

$$1 = \oint_C \frac{dh}{2\pi i} \{ \mathcal{H}_H(h) + \mathcal{F}(h) \} \quad (4.1)$$

which, along with the normalization $\int_0^a dh \rho_H(h) = 1$ of the spectral density, implies that

$$\oint_C dh \mathcal{F}(h) = 0 \quad (4.2)$$

Thus, at least for some range of the couplings \tilde{t}_q^* , the function $\mathcal{F}(h)$ will be analytic in a neighbourhood of the cut of $\mathcal{H}_H(h)$. This will be true so long as the Itzykson-Zuber integral does not undergo a phase transition which changes its analyticity features in the large- N limit. The equation (3.6) can be used to determine $\mathcal{F}(h)$ once the coupling constants of the dynamical triangulation are specified. The simplest choice is a power law variation of the couplings as the coordination numbers are varied,

$$q\tilde{t}_q^* = t^{q-1+p} \quad ; \quad t \in \mathbb{R}, p \in \mathbb{Z} \quad (4.3)$$

so that each vertex of the triangulated surface interacts with a strength proportional to t (with proportionality constant t^p) with each of its nearest neighbours.

This simple choice of vertex weights in the triangulation model allows us to study more precisely how the curvature matrix model represents features of the random surface sum, and to further demonstrate that the actual saddle-point localization of the partition function is not onto some configuration of Young tableau weights other than the mod 3 representations. It will also allow us to examine how the observables of the model behave as the weights are varied in this simple case, without the complexities that would appear in the analytic form of the solution for other choices of coupling constants. For generic $t \neq 1$ (i.e. $\mathcal{F}(h) \neq 0$), the saddle-point solution of the matrix model must satisfy certain physical consistency conditions so that it really does represent the (continuum) genus zero contribution to the random surface

sum (1.3) with the choice of couplings (4.3). Using Euler's theorem $V - E + F = 2$ for a spherical topology and the triangulation relation

$$\sum_{v_q^* \in G_3} q = 2E = 3F \quad (4.4)$$

it follows that the planar surface sum in (1.3) is

$$Z_H^{(0)}(\lambda, t) = t^{2(p-1)} \sum_{G_3^{(0)}} c_{G_3^{(0)}} \left(\lambda^3 t^{p+1} \right)^{A(G_3^{(0)})} \quad (4.5)$$

where the sum is over all planar fat-graphs $G_3^{(0)}$ of area $A(G_3^{(0)}) \propto F(G_3^{(0)})$, and the constant $c_{G_3^{(0)}}$ is independent of the coupling constants λ and t . The perturbative expansion parameter is $\lambda^6 t^{2(p+1)}$ and the critical point, where a phase transition representing the continuum limit of the discretized random surface model takes place, is reached by tuning the expansion parameter to the radius of convergence of the power series (4.5). The critical line $\lambda_c(t)$ thus obeys an equation of the form

$$\lambda_c(t)^6 \cdot t^{2(p+1)} = \text{constant} \quad (4.6)$$

The solution of the model for $t \neq 1$ should therefore have the same physical characteristics as that with $t = 1$, since in the random surface interpretation of the curvature matrix model the only effect of changing t is to rescale the cosmological constant of the random surface sum for $t = 1$ as $\lambda^3 \rightarrow \lambda^3 t^{p+1}$. This geometrical property should be reflected in the large- N solution of the matrix model with a non-vanishing Itzykson-Zuber correlator.

As discussed in [5], it is possible to invert the equation

$$G(h) = e^{\mathcal{H}_H(h) + \mathcal{F}(h)} \quad (4.7)$$

to obtain h as a function of G , by changing variables in the contour integral (3.6) from h to G to get

$$q\tilde{t}_q^* = \oint_{\mathcal{C}_G} \frac{dG}{2\pi i G} h(G) G^q \quad (4.8)$$

where the contour \mathcal{C}_G encircles the cut $[G(b), 0]$ with clockwise orientation in the complex G -plane. Then

$$h(G) = 1 + \sum_{q=1}^{\infty} \frac{q\tilde{t}_q^*}{G^q} + \sum_{q=1}^{\infty} g_q G^q \quad (4.9)$$

where the coefficients

$$g_q \equiv \oint_{\mathcal{C}_G} \frac{dG}{2\pi i G} h(G) G^{-q} = \lambda^{-q} \left\langle \frac{\text{tr}}{N} (X A_3)^{3q} \right\rangle_{\mathcal{M}_3^*} \quad (4.10)$$

determine the analytic part of the function $h(G)$. The second equality in (4.10) follows from (3.44) and the constant term in the Laurent series expansion (4.9) is unity because of the

normalization of the spectral density ρ_H [5]. In the general case, the solution for $G(h)$ as determined from (4.9) will be multi-valued. It was shown in [5] that the first set of sheets of the Riemann surface of this multi-valued function are connected along, and hence determined by, the cut structures of $e^{\mathcal{F}(h)}$, which map the point $h = \infty$ to $G = 0$. These sheets are found by inverting (4.9) with $g_q = 0$. The remaining sheets are determined by the cuts of $e^{\mathcal{H}_H(h)}$ and are associated with the positive powers of G in (4.9).

The solution is extremely simple, however, for the choice of couplings (4.3), as then the inversion of the equation (4.9) with $g_q = 0$ yields

$$G_1(h) = t + \frac{t^p}{h-1} \quad (4.11)$$

This solution has a simple pole of residue t^p at $h = 1$, but no multivalued branch cut structure. Thus we expect that the singularities of $e^{\mathcal{F}(h)}$ will have a pole structure, rather than a cut structure. The remaining sheets of the function $G(h)$ will be determined by the cut structure of $e^{\mathcal{H}_H(h)}$. They are attached to the ‘‘physical’’ sheet $G_1(h)$, on which the poles of $e^{\mathcal{F}(h)}$ and the cuts of $e^{\mathcal{H}_H(h)}$ lie, by these cuts. Note that the analytical structure of the character as determined by this part of the Laurent series in (4.9) is anticipated from the Schur character formula (3.9),(3.10).

With this observation we can in fact obtain a closed form expression for the Itzykson-Zuber correlator in the large- N limit, in contrast to the generic case [5] where in general one obtains only another discontinuity equation such as (3.3). The resolvent function (3.4) can be written as

$$\mathcal{H}_H(h) = \log\left(\frac{h}{h-b}\right) + \tilde{\mathcal{H}}_H(h) \quad (4.12)$$

where $\tilde{\mathcal{H}}_H(h) = \int_b^a dh' \rho_H(h')/(h-h')$ is the reduced resolvent function associated with the non-trivial part of the density ρ_H , and it has a branch cut on the interval $[b, a]$. Using (4.2) it can be written as

$$\tilde{\mathcal{H}}_H(h) = \oint_{\tilde{\mathcal{C}}} \frac{d\tilde{h}}{2\pi i} \frac{\log G(\tilde{h})}{h-\tilde{h}} = - \oint_{\mathcal{C}_G} \frac{dG}{2\pi i} \frac{h'(G)}{h-h(G)} \log G \quad (4.13)$$

where the contour $\tilde{\mathcal{C}}$ encircles the cut $[b, a]$ of $\tilde{\mathcal{H}}_H(h)$ and we have changed variables from h to G as above. The contour integral (4.13) in the complex G -plane can be evaluated for large- h , which, by analytical continuation, determines it for all h . We can shrink the contour \mathcal{C}_G down to an infinitesimal one \mathcal{C}_0 hugging both sides of the cut $[G(b), 0]$. In doing so, from (4.9) it follows that we pick up contributions from the solution (4.11) and the extra pole at $G = t$ corresponding to the point $h = \infty$. Thus integrating by parts we find that (4.13) can be written as

$$\tilde{\mathcal{H}}_H(h) = \log G_1(h) - \log t + \oint_{\mathcal{C}_0} \frac{dG}{2\pi i} \left\{ \frac{\partial}{\partial G} [\log G \log(h-h(G))] - \frac{1}{G} \log(h-h(G)) \right\} \quad (4.14)$$

In the contour integral over \mathcal{C}_0 in (4.14), the total derivative in G gives the discontinuity across the cut $[G(b), 0]$, which is $\log(h - b)$. The other term there evaluates the $G = 0$ limit of $\log(h - h(G))$ determined by (4.9) and (4.11). Using (4.12), we then have

$$\mathcal{H}_H(h) = \log G_1(h) + \log \left(\frac{h}{(h-1)t + t^p} \right) \quad (4.15)$$

Since there is only the single (physical) sheet determined by the singularity structure of $e^{\mathcal{F}(h)}$, we have $\log G_1(h) = \mathcal{F}(h) + \mathcal{H}_H(h)$ on the physical sheet, and combined with (4.15) we arrive at the expression

$$\mathcal{F}(h) = \log \left(\frac{(h-1)t + t^p}{h} \right) \quad (4.16)$$

for the large- N limit of the Itzykson-Zuber correlator. As mentioned above, the fact that $e^{\mathcal{F}(h)}$ has only a simple pole of residue $t^p - t$ at $h = 0$ is because there are no other sheets below $G_1(h)$ connected by cuts of $e^{\mathcal{F}(h)}$. This is opposite to the situation that occurs in the Gaussian case ($A = 0$ in (1.1)), where $e^{\mathcal{H}_H(h)}$ has a simple pole of residue 1 at $h = 1$ and there are no upper branches above $G_1(h)$ connected by cuts of $e^{\mathcal{H}_H(h)}$ [5]. It can be easily verified, by blowing up the contour \mathcal{C} , using the asymptotic boundary condition $\mathcal{H}_H(h) \sim 1/h + \mathcal{O}(1/h^2)$ for large- h and computing the residue at $h = \infty$ in (3.6), that (4.16) consistently yields the weights (4.3). Furthermore, for $p = t = 0$, (4.16) reduces to the solution of [5] in the case where only the vertex weight \tilde{t}_1^* is non-zero, while for $t = 1$ (i.e. $\bar{A} = \tilde{A} = \mathbf{1}$), (4.16) yields $\mathcal{F}(h) = 0$, as expected from its definition.

Notice that for $p \neq 1$, $\mathcal{F}(h)$ here has a logarithmic branch cut between $h = 0$ and $h = \bar{t} \equiv 1 - t^{p-1}$, so that strictly speaking the solution (4.16) is only valid for $\bar{t} \leq 0$, i.e. $0 \leq t \leq 1$ for $p \leq 0$ and $t \geq a$ for $p > 1$ (where its cut doesn't overlap with the cut $[0, a]$). Outside of this region the analytic structure of the Itzykson-Zuber correlator can be quite different. For $p = 1$, we have $\mathcal{F}(h) = \log t$ and the only effect of the Itzykson-Zuber integral in the saddle-point equation (3.3) is to rescale the cosmological constant as $\lambda^3 \rightarrow \lambda^3 t^2$. This is expected directly from the original matrix integral (1.1), since for $p = 1$ the vertex weights can be represented as traces of the external matrix $A = t \cdot \mathbf{1}$, while for $p \neq 1$ the $GL(N, \mathbb{C})$ characters can only be defined via the generalized Schur functions (3.9), (3.10). For $p \neq 1$, we shall now see that (4.16) changes the analytic structure of the large- N solution of the curvature matrix model, but that the $t = 1$ physical characteristics (the pure gravity continuum limit) are unchanged.

The saddle-point equation (3.3) with (4.16) is then solved by replacing the $t = 1$ resolvent $\mathcal{H}_H(h; \lambda^3, 1)$ in (3.27) by

$$\mathcal{H}_H(h; \lambda^3, t) = \mathcal{H}_H(h; \lambda^3, 1) + 2 \oint_{\mathcal{C}} \frac{ds}{2\pi i} \frac{1}{s-h} \sqrt{\frac{(h-a)(h-b)}{(s-a)(s-b)}} \log \left(\frac{(s-1)t + t^p}{s} \right) \quad (4.17)$$

and compressing the closed contour \mathcal{C} in (4.17) to the cut $[\bar{t}, 0]$. Note that since $\bar{t} \leq 0$ the sign of the square root in (4.17) is negative along this cut. Working out the contour integration in (4.17) as before then gives

$$\begin{aligned} \mathcal{H}_H(h; \lambda^3, t) &= \mathcal{H}_H(h; \lambda^3 t^{p+1}, 1) \\ &+ 2 \log \left\{ \frac{h^2 (h(a+b) - 2ab - \bar{t}(2h-a-b) - 2\sqrt{(h-a)(h-b)(\bar{t}-a)(\bar{t}-b)})}{(h-\bar{t})^2 (h(a+b) - 2ab - 2\sqrt{ab(h-a)(h-b)})} \right\} \end{aligned} \quad (4.18)$$

The endpoints a, b of the support of the spectral distribution function are found just as before and now the boundary conditions (3.28) are replaced by

$$\xi_t = \lambda^6 t^{2(p+1)} \eta_t^3 \quad , \quad 1 - \bar{t} = t^{p-1} = \eta_t - 3\xi_t \quad (4.19)$$

where

$$\xi_t = \frac{1}{4} \left(\sqrt{a-\bar{t}} - \sqrt{b-\bar{t}} \right)^2 \quad , \quad \eta_t = \frac{1}{4} \left(\sqrt{a-\bar{t}} + \sqrt{b-\bar{t}} \right)^2 \quad (4.20)$$

and we have assumed that $t \neq 0$ ¹.

The boundary equations (4.19) are identical to those of the $t = 1$ model in (3.28) with the replacements $\xi \rightarrow \bar{\xi}_t \equiv t^{1-p} \xi_t$, $\eta \rightarrow \bar{\eta}_t \equiv t^{1-p} \eta_t$ and $\lambda^3 \rightarrow \lambda^3 t^{p+1}$. The weight average $\langle h \rangle_t$ corresponding to the $1/h^2$ coefficient of the asymptotic expansion of (4.18) is then

$$\langle h \rangle_t = \frac{1}{2} + t^{2(p-1)} \left(-\frac{\bar{\eta}_t^2}{3} + \bar{\eta}_t - \frac{2}{3} \right) \quad (4.21)$$

where we have used (4.19). Substituting (4.21) into (3.33) yields (3.35) with $\eta \rightarrow \bar{\eta}_t$ and an additional overall factor of $t^{2(p-1)}$ which represents the overall factor in (4.5) (the linear in λ term is from the Gaussian normalization of the partition function). Thus, although the precise analytical form of the solution is different, the critical behaviour (and also the Wick expansion) of the curvature matrix model for the choice of vertex weights (4.3) with $t \neq 1$ is the same as that for $t = 1$.

The correlators (3.32) will all have a structure similar to those at $t = 1$, as in (4.21). The non-trivial analytical structure of the saddle-point solution for $t \neq 1$ is exemplified most in

¹It can be easily seen that for $p = t = 0$ the saddle-point equations are not satisfied anywhere. This simply reflects the fact that it is not possible to close a regular, planar triangular lattice on the sphere. As discussed in [4, 5], in the matrix model formulations one needs to study “almost” flat planar diagrams in which positive curvature defects are introduced on the Feynman graphs to close that triangular lattice on the sphere.

the function (4.7), which in the present case is

$$\begin{aligned}
G(h; \lambda^3, t) &= G(h; \lambda^3 t^{p+1}, 1) \\
&\times \frac{th^3 (h(a+b) - 2ab - \bar{t}(2h - a - b) - 2\sqrt{(h-a)(h-b)(\bar{t}-a)(\bar{t}-b)})^2}{(h-\bar{t})^3 (h(a+b) - 2ab - 2\sqrt{ab(h-a)(h-b)})^2} \\
&= \frac{(h(a+b) - 2ab - \bar{t}(2h - a - b) - 2\sqrt{(h-a)(h-b)(\bar{t}-a)(\bar{t}-b)})^2}{\lambda^3 t^p (\sqrt{a} + \sqrt{b})^2 (a-b)(h-\bar{t})^3 (h(a+b) - 2ab - 2\sqrt{ab(h-a)(h-b)})} \quad (4.22)
\end{aligned}$$

The inverse function $h(G)$ can be determined from (4.22) using the Lagrange inversion formula [9]

$$h(G) = G + \sum_{k=1}^{\infty} \frac{1}{k!} \left(\frac{\partial}{\partial G} \right)^{k-1} \varphi(G)^k \quad (4.23)$$

where the function φ is defined from (4.22) by

$$\varphi(h) = h - G(h) \quad (4.24)$$

Comparing with (4.9) for the choice of vertex weights (4.3), we can write down an expression for the generating function of the dual moments of the triangulation model (or equivalently for the 4-point and even-even models)

$$\sum_{q=1}^{\infty} \lambda^{-q} \left\langle \frac{\text{tr}}{N} (XA_3)^{3q} \right\rangle_{\mathcal{M}_3^*} G^q = G - \frac{t^{p-1}G}{G-t} + \sum_{k=1}^{\infty} \frac{1}{k!} \left(\frac{\partial}{\partial G} \right)^{k-1} \varphi(G)^k \quad (4.25)$$

Because of the complicated structure of the function (4.22), it does not seem possible to write down a closed form for this generating function or systematic expressions for the dual moments. Nonetheless, (4.25) does represent a formal solution for the observables of the triangulation model.

The above critical behaviour, when a non-trivial Itzykson-Zuber correlator is incorporated into the dynamical triangulation model, is anticipated from (4.6) and thus yields a non-trivial verification of the assumptions that went into the derivation of the large- N limit of the Itzykson-Di Francesco formula of section 2. The form of the function $G(h; \lambda^3, t)$ in (4.22) illustrates the analytical dependence of the saddle-point solution on the vertex weights \tilde{t}_q^* . It also demonstrates how the analytical, non-perturbative properties of the random surface sum (4.5) change at $N = \infty$, although the perturbative expansion of the free energy coincides with (4.5) and the physical continuum limit (4.6) is unaltered. The discussion of this section of course also applies to the 4-point and even-even models with the appropriate redefinitions of coupling constants above, and also to the complex curvature matrix model where now the incorporation of the Itzykson-Zuber correlator using the saddle-point equation (3.22) leads

to the appropriate rescaling of the cosmological constant $\lambda^{3/2}$ by $t^{(p+1)/4}$ as predicted from the graphical arguments of subsection 3.3 (see (3.24)). The above derivation also suggests an approach to studying phase transitions in the large- N limit of the Itzykson-Zuber model, as it shows in this explicit example the region where the analytic structure of $\mathcal{F}(h)$ changes (i.e. $\bar{t} > 0$) and consequently the region wherein a discontinuous change of the large- N solution appears. This could prove relevant to various other matrix models where the Itzykson-Zuber integral appears [7, 11]. The saddle-point solution above of the curvature matrix model can nonetheless be trivially analytically continued to all $t \in \mathbb{R}$. This is expected since the random surface sum (4.5) is insensitive to a phase transition in the Itzykson-Zuber integral which appears in the large- N solution of the matrix model only as a manifestation of the character sum representation of the discretized surface model.

5 Complex Saddle Points of the Itzykson-Di Francesco Formula

The curvature matrix models we have thus far studied have led to a unique, stable saddle-point solution at large- N . From the point of view of the Itzykson-Di Francesco formula of section 2, there is a crucial reason why this feature has occurred, namely the cancellation of sign factors that appear in expressions such as (2.2). The models we have studied have been arranged so that there is an overall cancellation of such sign factors which arise from the splitting of the Young tableau weights into the appropriate congruence classes. When the weights are then assumed to distribute equally the resulting Vandermonde determinant factors stabilize the saddle-point and lead to a unique real-valued solution for the free energy and observables of the random matrix model. In this section we shall briefly discuss the problems which arise when trying to solve the matrix models when the sign variation terms in the character expansion formulas do not necessarily cancel each other out.

The destabilization of the real saddle-point configuration of weights was pointed out in [4] where it was shown that the configuration is *complex* for the Hermitian one-matrix model with Penner potential [9]

$$V_P(XA) = -\log(\mathbf{1} - X) \quad (5.1)$$

in (1.1). The Itzykson-Di Francesco formula for this matrix model follows from replacing $\mathcal{X}_3[h]$ by $\chi_{\{h\}}(A) = \chi_{\{h\}}(\mathbf{1}) \propto \Delta[h]$ in (2.5), so that at $N = \infty$ we have

$$Z_P^{(0)} = c_N \lambda^{-N^2/4} \sum_{h=\{h^e, h^o\}} \Delta[h^o]^2 \Delta[h^e]^2 \prod_{i,j=1}^{N/2} (h_i^o - h_j^e) e^{\frac{1}{2} \sum_i h_i [\log(\frac{\lambda h_i}{N}) - 1]} \quad (5.2)$$

Now there is no problem with the decomposition of weights into the appropriate congruence classes, but, as we shall see below, the rapid sign changes of the mixed product over the even and odd weights destabilize the reality of the saddle-point configuration of Young tableau weights. In the previous models such mixed product factors did not pose any problem for the solution at large- N because they appeared in the denominators of the character expansions and acted to make the more probable configurations of weights those with identical distributions of even and odd weights, thus stabilizing the saddle-point at $N = \infty$. In (5.2), however, the mixed product $\prod_{i,j} (h_i^o - h_j^e)$ appears in the numerator and thus acts to make the more probable configuration those with different distributions of even and odd weights. Thus when a symmetric distribution over h_i^e and h_j^o in (5.2) is assumed, this has the effect of destabilizing the saddle-point leading to a complex-valued solution.

The matrix model with Penner potential (5.1) is equivalent to the standard Hermitian one-matrix model for pure gravity [1], i.e. that with potential $\frac{1}{4} \text{tr } X^4$ in (1.1). Diagrammatically, a two-to-one correspondence between planar Feynman graphs of these two matrix models exists by splitting the 4-point vertices of the X^4 model as described in subsection 3.2 to give diagrams of the “even-log” model with potential $-\log(\mathbf{1} - X^2) = -\log(\mathbf{1} - X) - \log(\mathbf{1} + X)$ (so that the face centers of the X^4 model are mapped onto the vertices and face centers of the even-log model). From the point of view of the Itzykson-Di Francesco formula, in the character expansion (2.5) for the X^4 model we replace $\mathcal{X}_3[h]$ by $\mathcal{X}_4[h]$. The resulting partition function Z_4 is a sum over mod 4 congruence classes of weights in which the distribution sums for the classes $\mu = 0, 2$ and $\mu = 1, 3$ decouple from each other (so that even and odd weights completely factorize) and each have the precise form at $N = \infty$ of the partition function (5.2) [4], i.e. $Z_4^{(0)} = (Z_P^{(0)})^2$. This is just the graphical correspondence mentioned above. Thus the Itzykson-Di Francesco formula at least reproduces correct graphical equivalences in these cases.

To see how the complex saddle-points arise in the character expansion of the Penner matrix model above, we assume that even and odd weights distribute symmetrically in (5.2) and define a distribution function $\rho_P(h)$ for the $N/2$ weights h_i^e . Varying the effective action in (5.2) for the weights h^e then leads to the large- N saddle-point equation

$$\int_b^a dh' \frac{\rho_P(h')}{h - h'} = -\frac{1}{3} \log(\lambda h) - \log\left(\frac{h}{h - b}\right) \quad , \quad h \in [b, a] \quad (5.3)$$

The corresponding resolvent function $\mathcal{H}_P(h)$ can be determined by the contour integration in (3.26) just as before using (5.3) and we find after some algebra

$$\mathcal{H}_P(h) = \frac{1}{3} \log \left\{ \frac{(\sqrt{a} - \sqrt{b})^2(a - b)}{\lambda} \frac{h \left(h + \sqrt{ab} + \sqrt{(h - a)(h - b)} \right)^2}{\left(h(a + b) - 2ab + 2\sqrt{ab(h - a)(h - b)} \right)^3} \right\} \quad (5.4)$$

Expanding (5.4) for large- h then leads to the boundary conditions

$$\xi = \frac{3}{5}(\eta - 1) \quad , \quad \left(\frac{5}{3}\right)^3 \lambda^2 \eta^5 = (\eta - 1)^3 \quad (5.5)$$

Consider the structure of the solutions to the boundary conditions (5.5). Again, the Wick expansion of the original matrix integral is analytic about $\lambda = 0$, and it can be shown that the free energy is analytic about $\eta(\lambda = 0) = 1$. We should therefore choose the branches of the quintic equation in (5.5) which are regular at $\lambda = 0$. There are three solutions which obey this analyticity condition and they are given by the iterative relations

$$\eta_n = 1 + \frac{5}{3} \omega_3^n \lambda^{2/3} (\eta_n)^{5/3} \quad , \quad n = 0, 1, 2 \quad (5.6)$$

where $\omega_3 \in \mathbb{Z}_3$ is a non-trivial cube root of unity. The remaining two solutions behave near $\lambda = 0$ as $\eta \sim \pm \lambda^{-1}$. The discrete \mathbb{Z}_3 -symmetry of the regular saddle-point solutions (5.6) seems to be related to the fact that the Schwinger-Dyson field equations of this matrix model determine the function $G_P(h) = e^{\mathcal{H}_P(h)}$ as the solution of a third-order algebraic equation [4]

$$\lambda h^3 G_P^3 - \lambda h^2 (1 + h) G_P^2 + \left[\frac{8}{9} - h + \frac{1}{648\lambda} (1 - \sqrt{1 - 12\lambda}) (1 - 12\lambda) \right] h G_P + h^2 = 0 \quad (5.7)$$

Initially, the endpoints a, b of the support of the spectral density lie on the positive real axis, so that one expects that only the real branch η_0 is a valid solution of the matrix model. However, the perturbative expansion parameter of the free energy $S_P(\eta_0)$ would then be $\lambda^{2/3}$. It is easy to see by a Wick expansion of the original matrix integral that the genus zero expansion parameter is in fact λ^2 . Furthermore, one can analyse the analytic properties of the solutions to the quintic boundary equation in (5.5), and even determine the critical point λ_c which in this case is the point where the two real and positive roots coalesce. For $\lambda > \lambda_c$ all three roots which are analytic about $\lambda = 0$ become complex-valued. This critical behaviour is similar to that discussed for the cubic boundary equation (3.28) in subsection 3.4, and so apparently lies in the same universality class as the earlier models. However, the critical value λ_c determined this way does not agree with known results [1, 16], so that the free energy S_P determined from the character expansion does not count the Feynman graphs of the Penner model correctly.

The structure of complex saddle-points arises in many other matrix models. For example, for the quartic-type Penner potential

$$V_P^{(4)}(XA) = -\log(\mathbf{1} - X^4) \quad (5.8)$$

the boundary conditions determining the endpoints a, b of the support of the distribution function are

$$\xi = \frac{3}{7}(\eta - 1) \quad , \quad \left(\frac{7}{3}\right)^3 \lambda^4 \eta^7 = (\eta - 1)^3 \quad (5.9)$$

Again, there are three regular solutions of (5.9) at $\lambda = 0$ and the real root leads to an expansion in $\lambda^{4/3}$, whereas the Wick expansion can be explicitly carried out and one finds that the perturbative expansion parameter is λ^4 .

All the models we have studied for which the matrix model saddle point does not reproduce the graphical expansion share the feature that the constraint of regularity at $\lambda = 0$ yields multiple solutions of the endpoint equations. Choosing the real root (or any other single root) leads to the wrong solution of the matrix model. Thus it appears that the saddle-point should be defined by some kind of analytical continuation that extends the support of the spectral density ρ_P into the complex plane and takes proper account of the multiple root structure. It would be interesting to resolve these problems and determine the general technique for dealing with such complex saddle-points. It would also be interesting to discover any connection between this saddle-point destabilization and the well-known occurrence of (single-branch) complex saddle points for the eigenvalue distributions in generalized Penner models [16].

6 Conclusions

In this paper we have shown that the character expansion techniques developed in [4, 5] can be applied to odd potentials. We have demonstrated that the splitting of weights into congruence classes other than those of the even representations of $GL(N, \mathbb{C})$ leads to a proper solution of the matrix model, provided that one writes the weight distribution that appears in the character expansion over the appropriate congruence elements. The Itzykson-Di Francesco formula then correctly reproduces relations between different models.

From a mathematical perspective, the results of this paper raise some questions concerning the large- N limit of the Itzykson-Di Francesco formula. For instance, a random surface model with a discrete \mathbb{Z}_p -symmetry corresponding to, say, a p -colouring of its graphs will be described by a curvature matrix model with the \mathbb{Z}_p -symmetry $A \rightarrow \omega_p A$, $\omega_p \in \mathbb{Z}_p$. This symmetry will be reflected in the Itzykson-Di Francesco expansion as a localization of the group character sum onto mod p congruence class representations of $GL(N, \mathbb{C})$. The appropriate solution of the model at $N = \infty$ will then involve resumming the Young tableau weights over the mod p congruence classes and assuming that the even-odd decomposition factorizes symmetrically over these classes. However, it is not immediately clear why such a symmetry assumption of the character expansion at large- N gives the appropriate solution of the discretized planar surface theory (although a mapping onto a complex matrix model indicates how this should work). At this stage there seems to be a mysterious “hidden” symmetry at play which makes the large- N group theoretical approach to solving these random surface models work. Furthermore, other intriguing features of the Itzykson-Di Francesco formula,

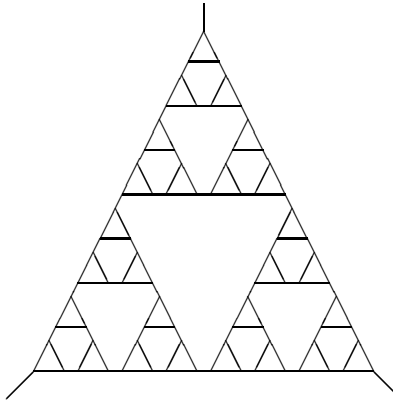


Figure 5: An example of a regular fractal-type graph that appears in the dynamical triangulation.

such as the appearance of phase transitions in the Itzykson-Zuber integral represented through the large- N limit of generalized Schur functions, are purely a result of the character expansion representation and correctly conspire to yield the proper solution of the random surface model. It would be interesting to put all of these features into some systematic framework for dealing with curvature matrix models in general.

From a physical point of view, there are many random surface models which are best dealt with using the dynamical triangulations studied in this paper, and it would be interesting to exploit the relationships with the even coordination number models to study the properties of these theories. For instance, one sub-ensemble of the random surface sum (1.3) is the collection of regular fractal-like graphs (Fig. 5) which were shown in [17] to dominate, in the high-temperature limit, the surface sum for two-dimensional quantum gravity coupled to a large number of Ising spins when restricted to two-particle irreducible Feynman diagrams. These fractal graphs can be characterized by 3-point graphs G_3 where only the dual coordination numbers

$$q_k^* = 3 \cdot 2^k \quad , \quad k \geq 0 \quad (6.1)$$

are permitted. Here k is the order of the fractal construction obtained inductively by replacing each 3-point vertex of an order $k - 1$ fractal graph with a triangle². The ensemble of fractal graphs corresponds to a branched polymer phase of two-dimensional quantum gravity [6]. We have shown that when the $3m$ -sided polygons in (1.3) are weighted with a power law variation with the number of sides, the continuum limit of the model lies in the pure gravitational phase.

²Note that the total number of triangle sides along each outer side of the fractal-like structure of a single, order $k + 1$ fractal graph is $2^k - 1$. Thus to be able to close the set of 3-point graphs of dual coordination numbers (6.1) on a spherical topology (corresponding to $N = \infty$ in the matrix model), one needs to glue an order k and an order $k + 1$ fractal graph together along their three external corner legs (see Fig. 5) so that the valence of the dual vertices of the faces joining the two fractal structures will coincide with (6.1).

The curvature matrix model (1.1) with the dual vertex weights arranged as discussed in this paper can thus serve as an explicit model for the transition from a theory of pure random surfaces (associated with central charge $D < 1$) to a model of branched polymers (associated with $D \geq 1$). This might help in locating the critical dimension $D_c \geq 1$ where the precise branched polymer transition takes place.

References

- [1] P. Di Francesco, P. Ginsparg and J. Zinn-Justin, Phys. Rep. **254** (1995), 1
- [2] S.R. Das, A. Dhar, A.M. Sengupta and S.R. Wadia, Mod. Phys. Lett. **A5** (1990), 1041
- [3] L. Chekhov and Yu. Makeenko, Mod. Phys. Lett. **A7** (1992), 1223
- [4] V.A. Kazakov, M. Staudacher and T. Wynter, Commun. Math. Phys. **177** (1996), 451
- [5] V.A. Kazakov, M. Staudacher and T. Wynter, Commun. Math. Phys. **179** (1996), 235
- [6] J. Ambjørn, B. Durhuus, J. Fröhlich and P. Orland, Nucl. Phys. **B270** [FS16] (1986), 457;
J. Ambjørn, B. Durhuus and T. Jónsson, Phys. Lett. **B244** (1990), 403; Mod. Phys. Lett. **A9** (1994), 1221;
J. Ambjørn, B. Durhuus, T. Jónsson and G. Thorleifsson, Nucl. Phys. **B398** (1993), 568
- [7] Yu. Makeenko, Nucl. Phys. **B49** (Proc. Suppl.) (1996), 226
- [8] V.A. Kazakov, M. Staudacher and T. Wynter, Nucl. Phys. **B471** (1996), 309
- [9] P. Di Francesco and C. Itzykson, Ann. Inst. Henri Poincaré **59** (1993), 117
- [10] C. Itzykson and J.-B. Zuber, J. Math. Phys. **21** (1980), 411
- [11] D.J. Gross, Phys. Lett. **B293** (1992), 181;
S. Khokhlachev and Yu. Makeenko, Phys. Lett. **B297** (1992), 345;
A.A. Migdal, Mod. Phys. Lett. **A8** (1993), 153; 359;
Yu. Makeenko, Intern. J. Mod. Phys. **A10** (1995), 2615;
G.W. Semenoff and R.J. Szabo, to be published in Intern. J. Mod. Phys. **A** (1997)
- [12] V.A. Kazakov, M. Staudacher and T. Wynter, in *Low Dimensional Applications of Quantum Field Theory*, Proc. 1995 Cargese Summer School (1996), to appear
- [13] M.R. Douglas and V.A. Kazakov, Phys. Lett. **B319** (1993), 219
- [14] J. Ambjørn, L. Chekhov, C.F. Kristjansen and Yu. Makeenko, Nucl. Phys. **B404** (1993), 127
- [15] M.J. Bowick, S.M. Catterall and G. Thorleifsson: Minimal Dynamical Triangulations of Random Surfaces, Syracuse preprint SU-4240-632 (1996)
- [16] C.-I. Tan, Mod. Phys. Lett. **A6** (1991), 1373;
S. Chaudhuri, H.M. Dykstra and J.D. Lykken, Mod. Phys. Lett. **A6** (1991), 1665;
J. Ambjørn, C.F. Kristjansen and Yu. Makeenko, Phys. Rev. **D50** (1994), 5193
- [17] M.G. Harris and J.F. Wheater, Nucl. Phys. **B427** (1994), 111